Monthly Notices
of the
ROYAL ASTRONOMICAL SOCIETY

Mon. Not. R. Astron. Soc. **420,** 3451–3468 (2012) doi:10.1111/j.1365-2966.2011.20276.x

Constraining the physical properties of Type II-Plateau supernovae using nebular phase spectra

K. Maguire,[1,2⋆] A. Jerkstrand,[3] S. J. Smartt,[2] C. Fransson,[3] A. Pastorello,[4] S. Benetti,[4] S. Valenti,[4] F. Bufano[5] and G. Leloudas[6]

[1]*Department of Physics (Astrophysics), University of Oxford, DWB, Keble Road, Oxford OX1 3RH*
[2]*Astrophysics Research Centre, School of Maths and Physics, Queen's University Belfast, Belfast BT7 1NN*
[3]*Department of Astronomy, The Oskar Klein Centre, Stockholm University, SE-106 91 Stockholm, Sweden*
[4]*INAF Osservatorio Astronomico di Padova, Vicolo dell'Osservatorio 5, 35122 Padova, Italy*
[5]*INAF Osservatorio Astronomico di Catania, Via S. Sofia 78, 95123 Catania, Italy*
[6]*Dark Cosmology Centre, Niels Bohr Institute, University of Copenhagen, Juliane Maries Vej 30, 2100 Copenhagen, Denmark*

Accepted 2011 November 25. Received 2011 November 23; in original form 2011 October 22

ABSTRACT

We present a study of the nebular phase spectra of a sample of Type II-Plateau supernovae with identified progenitors or restrictive limits. The evolution of line fluxes, shapes and velocities is compared within the sample, and interpreted by the use of a spectral synthesis code. The small diversity within the data set can be explained by strong mixing occurring during the explosion, and by recognizing that most lines have significant contributions from primordial metals in the H envelope, which dominates the total ejecta mass in these types of objects. In particular, when using the [O I] 6300, 6364 Å doublet for estimating the core mass of the star, care has to be taken to account for emission from primordial O in the envelope. Finally, a correlation between the Hα line width and the mass of ^{56}Ni is presented, suggesting that higher energy explosions are associated with higher ^{56}Ni production.

Key words: line: formation – line: profiles – radiative transfer – supernovae: general.

1 INTRODUCTION

Supernovae (SNe) are responsible for the production of most of the heavy elements that we observe in the Universe today. In a core-collapse SNe (CC-SNe), this nucleosynthesis occurs both by hydrostatic burning during the star's evolution and by explosive burning behind the shock after collapse. Woosley & Weaver (1995) analysed the yields of elements that are synthesized in massive stars and concluded that stars of 15–25 $M_\odot$ are the typical stars responsible for producing heavy elements. However, the initial mass function shows that low mass stars are more common, and therefore, depending on stellar yields, stars in the range 8–15 $M_\odot$ could also make a non-negligible contribution to the chemical enrichment of the Universe.

Type II-Plateau (IIP) SNe are a subset of CC-SNe, which result from the core collapse of massive H-rich stars, and therefore display prominent H features in their spectra, along with an extended plateau of nearly constant luminosity in their light curves. They are the most common supernova (SN) type making up ∼40 per cent of all SNe per unit volume (Smartt et al. 2009). Stellar evolutionary models predict that stars in the range 8–30 $M_\odot$ should explode as red supergiants (Heger et al. 2003; Limongi & Chieffi 2003; Eldridge & Tout 2004; Hirschi, Meynet & Maeder 2004). However, the progenitors of some IIP SNe have been identified, and apart from a few rare cases of blue supergiant progenitors (Walborn et al. 1987; Pastorello et al. 2005; Kleiser et al. 2011), they have been found to be red supergiants in a lower than expected mass range of 8–17 $M_\odot$ (Smartt et al. 2009). Utrobin & Chugai (2008, 2009) have modelled the light curves and spectral evolution of IIP SNe (some with progenitor identifications) and find larger masses of the exploding stars than those from the direct detections of the progenitors. This discrepancy between the progenitors obtained from direct imaging and those from modelling has also been analysed and discussed in Smartt et al. (2009) and Maguire et al. (2010) using a sample of nearby IIP SNe. One way of studying this discrepancy is to investigate and compare the nucleosynthetic yields from IIP SNe with identified progenitors.

We do this by studying a sample of IIP SNe at epochs when we can see emission from newly synthesized heavy elements. During the plateau phase of the light curve, which generally lasts for ∼80–120 d, the light curve is powered by remission of the energy deposited by the shock wave, including H recombinations. At these times, the H envelope is optically thick and we cannot see emission from the metal core. However, after the H has recombined, the envelope becomes transparent and the core becomes visible. The light

⋆E-mail: kate.maguire@astro.ox.ac.uk

curve then enters the radioactive decay phase, which is powered by the decay of ^{56}Co to ^{56}Fe. Radiative transfer effects are still significant in this phase, but decrease with time as the line optical depths fall. On the other hand, after approximately two years, the SNe generally become too faint to obtain good signal-to-noise spectra. Therefore, the optimal window for studying and interpreting the nucleosynthesis that has occurred is between one and two years post-explosion.

Very few IIP SNe have been studied in detail during the nebular phase and few late-time nebular spectra of IIP SNe exist, with the notable exception of SN 1987A, which due to its proximity was very well monitored. This lack of late-time spectral data is partly due to the long exposure times that are required to obtain sufficient signal-to-noise. The best observed IIP SNe at the necessary late times are SN 1987A (e.g. Phillips et al. 1990; Bouchet & Danziger 1993; Meikle et al. 1993; Wooden et al. 1993), SN 1990E (Benetti et al. 1994), SN 1999em (Leonard et al. 2002; Elmhamdi et al. 2003a), SN 2004et (Sahu et al. 2006; Maguire et al. 2010), SN 2007it (Andrews et al. 2011) and SN 2007od (Andrews et al. 2010; Inserra et al. 2011).

It is generally assumed that the emission lines of specific elements are emitted from regions containing predominantly those particular elements, i.e. that the O zone (formed in the late stages of pre-SN evolution or during the SN explosion) would be responsible for the production of the O emission lines. However, the final H envelope mass for an 8–12 $M_{\odot}$ star is ∼6–8 $M_{\odot}$ (e.g. Hirschi et al. 2004), much larger than the mass of synthesized metals of ∼0.5 $M_{\odot}$, and it is not clear if emission by primordial metals in the envelope may dominate that of synthesized ones. This has been shown by Li & McCray (1993a) to be the case in SN 1987A for the [Ca II] 7291, 7323 Å and the Ca II 8600 Å triplet, which are produced by a primordial abundance of Ca in the inner (velocity $< 2500\,\mathrm{km\,s^{-1}}$) region of the H and He envelope and not by newly synthesized Ca. Ca emission lines are very efficient cooling lines, and so even small quantities of primordial Ca can result in prominent emission lines in the late-time spectra (Fransson & Chevalier 1989). To obtain the observed flux of the Ca lines, Li & McCray (1993a) needed only a Ca mass of 2×10^{-4} $M_{\odot}$ in ∼5 $M_{\odot}$ of H in the inner envelope of SN 1987A, a factor of 10 times lower than that typically predicted for newly synthesized Ca in a SN 1987A-type progenitor star. Using models that included realistic mixing of the nuclear burning zones, Kozma & Fransson (1998a) showed that for SN 1987A, the Ca II 8600 Å triplet was at all times formed by emission from primordial Ca in the envelope, whereas the [Ca II] 7291, 7323 Å lines were formed by both synthesized and primordial Ca until ∼400 d, but mainly by primordial Ca after that.

This does not imply that there is no newly synthesized Ca but instead that if it is present at late times, the zones in which it is formed are too small and it cannot capture enough of the radioactive energy to create any strong emission, unless it is mixed with a greater mass of other elements such as H and He (Li & McCray 1993a).

Therefore, to calculate the relative emission strengths from primordial and synthesized material, the deposited energy in the different zones and the dominant processes responsible for the production of these lines must be modelled using a spectral synthesis code. Then the synthesized mass of O, Ca and Fe can be estimated by first subtracting the emission contribution from primordial material in the envelope. Previous studies of samples of CC-SN nebular phase spectra have mainly focused on stripped envelope SNe [Type Ib (lacking H) and Type Ic (lacking H and He)] (e.g. Maeda et al. 2008; Modjaz et al. 2008; Taubenberger et al. 2009; Milisavljevic et al. 2010) and have studied the [O I] 6300, 6364 Å profiles to look for possible signs of ejecta asphericity in the line profile shapes and how they evolve with time. Elmhamdi (2011) has studied a sample of CC-SNe including IIP SNe as well Type Ib/c SNe, focusing again on an analysis of the [O I] 6300, 6364 Å doublet. Using the overall luminosity of the [O I] doublet and the ratio of the two components, he has estimated the synthesized O mass, assuming that all the O luminosity is produced by freshly made O and not from primordial O in the envelope. We will show that this is a questionable assumption.

In this paper, we study a sample of 35 late-time nebular phase spectra of nine IIP SNe with identified progenitors to investigate how their spectral features change as a function of time, and how the flux, profile shape and velocity of the features vary among SNe. This can then be linked to the material distribution and physical conditions in the SNe. We will apply a spectral synthesis model to the nebular phase spectra to study line flux ratios and interpret their evolution with time as well as their internal differences. This paper is complemented by Jerkstrand et al. (in preparation), which derives detailed nucleosynthesis results for one of the SNe in the sample, SN 2004et, by a complete analysis of the spectral evolution from the ultraviolet (UV) to far-infrared.

2 SUPERNOVA SAMPLE OF NEBULAR SPECTRA

As mentioned in Section 1, the current sample of IIP SNe with multi-epoch optical spectra at late times is limited to a small number of objects. In particular, we wanted to focus on SNe with information available about their progenitor stars and ^{56}Ni mass estimates. To increase this sample, observations were obtained of four IIP SNe at the 3.6-m New Technology Telescope (NTT) with the European Southern Observatory (ESO) Faint Object Spectrograph and Camera version 2 (EFOSC2) in low-resolution spectroscopy mode and at the 8.2-m Very Large Telescope (VLT) with FOcal Reducer and low dispersion Spectrograph 2 (FORS2). The SNe observed were SNe 2007aa, 2008bk, 2008cn and 2009N at epochs spanning ∼360–550 d post-explosion. In addition to the new data set, the literature was searched for late-time nebular spectra of IIP SNe with progenitor information (either a progenitor has been identified in pre-explosion images or an upper mass limit has been set) and data from the following SNe were included: SNe 1987A, 1999em, 2003gd, 2004et and 2005cs. The complete sample of spectra analysed here is detailed in Table 1. All the spectra have been corrected for Galactic and host galaxy extinction using the values given in Table 2 and they have also been corrected to the rest frame of their respective host galaxies. The resolution of the spectra that are quoted was either taken from the literature or estimated from the full width at half-maximum (FWHM) of the night sky lines.

The ^{56}Ni masses and zero-age main-sequence masses of the SN progenitors, where available, are given in Table 2. The properties of the sample range from low-luminosity, low ^{56}Ni mass events such as SNe 2005cs, 2008bk and 2009N to higher luminosity, higher ^{56}Ni mass events such as SNe 1987A, 1999em and 2004et. However, the range in main-sequence masses listed in Table 2 does not show as large a spread between over- and under-luminous events, with the masses clustering at the lower end of the range expected from stellar evolutionary theory (8–30 $M_{\odot}$). We will investigate here if there are any measurable differences between the spectral properties of the IIP SNe in the sample and then determine how these differences might relate to their progenitor and explosion properties.

Table 1. Spectral observations of the sample of IIP SNe studied, including epoch, wavelength range, resolution and source of the spectrum. The SNe for which new data are presented in this paper are noted as VLT+FORS2 and NTT+EFOSC2 as well as the grism with which they were taken, as discussed in Section 2.

SN	Epoch (d)	λ Range (Å)	Resolution (Å)	Source
1987A	338	3110–10 930	16	Phillips et al. (1990)
	345	3100–10 610	16	Phillips et al. (1990)
	374	5160–10 690	16	Phillips et al. (1990)
	398	3200–10 220	16	Phillips et al. (1990)
	407	3020–7780	16	Phillips et al. (1990)
	422	3070–10 740	16	Phillips et al. (1990)
	497	3000-10 990	16	Phillips et al. (1990)
	513	3030–10 970	16	Phillips et al. (1990)
	525	3000–10 990	16	Phillips et al. (1990)
	529	4000–10 350	16	Asiago Supernova Archive
	586	3230–7500	16	Phillips et al. (1990)
	598	3830–10 170	16	Asiago Supernova Archive
1999em	312	3350–10 620	21	Elmhamdi et al. (2003a)
	319	3410–7770	21	Elmhamdi et al. (2003a)
	391	3500–9110	10	Elmhamdi et al. (2003a)
	465	3360–10 620	20	Elmhamdi et al. (2003a)
	510	3560–9240	10	Elmhamdi et al. (2003a)
	642	4200–9940	28	Elmhamdi et al. (2003a)
2003gd	493	4200–9600	13	Hendry et al. (2005)
2004et	284	4000–7820	36	Maguire et al. (2010)
	301	4000–8450	7	Sahu et al. (2006)
	314	4000–8450	7	Sahu et al. (2006)
	341	3400–8020	13	Maguire et al. (2010)
	384	3500–7750	24	Maguire et al. (2010)
	401	4000–8450	7	Sahu et al. (2006)
	408	4000–7730	25	Maguire et al. (2010)
	427	4000–8450	7	Sahu et al. (2006)
	464	4000–8450	7	Sahu et al. (2006)
2005cs	333	5050–10 470	18	Pastorello et al. (2009)
2007aa	376	4300–9600	10	VLT+FORS2+300V
2008bk	524	3500–9500	14	NTT+EFOSC2+gr#11[a]
	547	3800–9500	10	VLT+FORS2+300V
2008cn	358	3500–9500	10	VLT+FORS2+300V
2009N	366	6000–10 100	14	NTT+EFOSC2+gr#16[a]
	406	3500–9600	10	VLT+FORS2+300V

[a]The resolution of the gr#16 and gr#14 gratings is very similar but gr#16 is centred at a longer wavelength than gr#11.

Table 2. Some of the derived properties for the sample of IIP SNe analysed in this paper including their extinction, distance, ^{56}Ni mass and zero-age main-sequence (ZAM) mass.

SN	$E(B-V)$	Distance (Mpc)	Ni^{56} mass ($M_\odot$)	ZAM ($M_\odot$)	Source
1987A	0.19	49.9×10^{-3}	0.075 ± 0.005	14–20	1, 2
1999em	0.06	11.7 ± 1.0	0.042	<15	3
2003gd	0.14	9.3 ± 1.8	0.016	7^{+6}_{-2}	4
2004et	0.41	5.9 ± 0.4	0.064 ± 0.04	8^{+5}_{-1}	5, 6, 7
2005cs	0.05	8.4 ± 1.0	0.003	8 ± 2	8, 9, 10
2007aa	0.014	20.5 ± 2.6	–	<12	11, 12
2008bk	0.3	3.9 ± 0.4	0.004	9^{+4}_{-1}	13, 14
2008cn	0.35	33.3 ± 0.2	–	13 ± 2	15, 16
2009N	0.15	12.6 ± 0.9	0.009 ± 0.004	<16	16, 17

References: (1) Phillips et al. (1990); (2) Smartt (2009); (3) Elmhamdi et al. (2003a); (4) Hendry et al. (2005); (5) Sahu et al. (2006); (6) Maguire et al. (2010); (7) Crockett et al. (2011); (8) Maund, Smartt & Danziger (2005); (9) Li et al. (2006); (10) Pastorello et al. (2009); (11) Smartt et al. (2009); (12) Chornock et al. (2010); (13) Mattila et al. (2008); (14) van Dyk et al. (2012); (15) Elias-Rosa et al. (2009); (16) Fraser et al. (in preparation); (17) Takáts et al. (in preparation).

3 DESCRIPTION OF THE RADIATIVE TRANSFER MODEL

Full details of the spectral synthesis model used to study the nebular phase spectra can be found in Jerkstrand, Fransson & Kozma (2011) and Jerkstrand et al. (in preparation). Here we describe only the basic setup of the model and its important input parameters. The model uses as an input the $12\,M_{\odot}$ explosion model of a solar metallicity progenitor taken from Woosley & Heger (2007). A $12\,M_{\odot}$ model is chosen because this mass is typical of the progenitor mass estimates obtained from pre-explosion images of the sites of IIP SNe and stellar evolutionary models (Smartt et al. 2009, and references therein). The late stellar evolution and explosion of stars less massive than $12\,M_{\odot}$ involve significant uncertainties, and few if any useful models are available. In Jerkstrand et al. (in preparation) we discuss models for a wider set of masses.

The ejecta is divided into a spherically symmetric core and a spherically symmetric envelope, with the core containing the zones of the heavier elements (Fe/He, Si/S, O/Si/S, O/Ne/Mg, O/C), along with 15 per cent of the mass of H and 60 per cent of the mass of He mixed in from the envelope. The zones making up the core region are broken into clumps (100 for each zone), with the clumps of each zone having the same density and being randomly distributed throughout the core region. This simulates macroscopic mixing in the core and removes the rigid shell-like structure that is known to be not an accurate representation of the ejecta structure post-explosion, as will be discussed in Section 4. We allocate the filling factors using the same method as in Jerkstrand et al. (2011), assuming the same density for the synthesized O as derived for SN 1987A by Li & McCray (1992). At epochs in the range 100–1000 d post-explosion, the main source of luminosity is due to the radioactive decay of ^{56}Co and its mass can be constrained by measuring the bolometric luminosity during the radioactive tail phase of the SN. For this $12\,M_{\odot}$ model, a ^{56}Ni mass of $0.064\,M_{\odot}$ and a core velocity of $1800\,km\,s^{-1}$ were chosen to agree with the values obtained from observations of SN 2004et. The model computes the deposition of gamma rays and positrons, followed by iterative solutions to the equations of statistical and thermal equilibrium, as well as the radiation field. See Jerkstrand et al. (2011) for more details. We note that for low-velocity/low ^{56}Ni mass SNe such as SN 2008bk, the conditions for the steady-state calculation assumed in the model may not be met at all times, and the model line fluxes are therefore of limited accuracy for these types of SNe.

4 LINE PROFILE ANALYSIS

Standard stellar evolution models of massive stars (e.g. Woosley & Weaver 1995; Thielemann, Nomoto & Hashimoto 1996; Hirschi, Meynet & Maeder 2004) describe how the pre-explosion structure of the progenitor has an ordering of layers of elements from each nuclear burning stage, with the outermost layer being H and the innermost Fe. In the absence of mixing, this onion-layer structure would hold for SNe after explosion, and so if the emission of each particular element is formed in a different shell containing predominantly that element, then there would be a correlation between the elemental mass numbers and the width of their emission lines. The lightest elements (H, He) would have broad lines with pronounced flat tops, and the heaviest elements (Si, Si, Fe, Ni, Co) would have narrow lines. At the other extreme, if the elements are distributed uniformly throughout a sphere, then the line profiles would be parabolic in shape.

Studies of the observational properties of SN 1987A have found very similar line widths for a wide range of elements with no flat tops, which suggests extensive mixing of the ejecta (Fransson & Chevalier 1987; Meikle et al. 1989, 1993). This is supported by the early detection of gamma rays and X-rays from SN 1987A (Dotani et al. 1987; Sunyaev et al. 1987), which would occur only if ^{56}Co and ^{57}Co were mixed out into the inner envelope in concentrated clumps (Pinto & Woosley 1988; Kumagai et al. 1989). The detection of a high excitation line, He I 10 830 Å, at times greater than 10 d (Elias et al. 1988) would also occur only if it were reionized by gamma rays emitted in the He zones from outward mixed, decaying ^{56}Co (Graham 1988; Fassia et al. 1998).

4.1 Line profile shapes

Here we investigate the shapes of the profiles of the nebular phase emission lines in multi-epoch spectra for our sample of SNe, to study the distribution of elements in velocity space, and determine if signatures of mixing are also seen in the spectra of our sample. Fig. 1 shows the velocity profiles of the prominent emission lines present in SN 2004et at 300–464 d, while Fig. 2 shows the velocity profiles for SN 1999em in the range 312–510 d, and Fig. 3 shows the profiles for low-luminosity SNe 2008bk (524, 547 d) and 2009N (366, 406 d). The lines shown are Hα, [O I] 6300, 6364 Å, [Ca II] 7291, 7323 Å and [Fe II] 7155, 7172 Å. Each of the lines shown has had a linear continuum subtracted and has been normalized to its peak value. The [O I], [Ca II] and [Fe II] lines are doublets, and to compare the emission line shapes, the profiles have been centred on the rest wavelength of the blue components of the doublets.

None of the emission lines of these SNe shown in Figs 1,2 and 3 has a flat-topped profile at any epoch and the lines are instead roughly Gaussian in shape. However, the convolution of the emission lines with the point spread function of the instrument could result in a roughly Gaussian shape being seen for an intrinsically flat-topped profile if the intrinsic width of the line is smaller than or comparable to the resolution of the instrument. To investigate the effect, we have convolved a flat-topped profile (with the width of the Hα line) with a Gaussian (with the width of the instrumental resolution). However, before doing this, the observed FWHM ($\mathrm{FWHM_{obs}}$) must be corrected to account for the resolution of the instrument ($\mathrm{FWHM_{instr}}$) as measured from the FWHM of the night sky lines in each of the spectra to obtain the original width of the line before convolution with the telescope instrument. The corrected FWHM is given by

$$\mathrm{FWHM_{corr}} = \sqrt{\mathrm{FWHM_{obs}^2} - \mathrm{FWHM_{instr}^2}}. \quad (1)$$

Then for each SN in the sample, we convolved a flat-topped line profile (with the width of the Hα line, corrected for the instrumental resolution) with a Gaussian (with the width of the instrumental resolution) to determine if any of the line profiles were flat topped.

To demonstrate this, in Fig. 4, a comparison of the convolution of the resolution of the instrument with both a flat-topped and Gaussian profile is shown for two different $\mathrm{FWHM_{corr}}$ values. In the top panel of Fig. 4 using an $\mathrm{FWHM_{corr}}$ of 20 Å, it is not possible to distinguish from the output between the two scenarios. However, in the bottom panel with an $\mathrm{FWHM_{corr}}$ value of 28 Å, the result is different, with the flat-topped profile giving a broader, flatter-topped line profile. The FWHM at which it becomes difficult to distinguish between the intrinsic profile types for the quoted resolutions is ∼29 Å for the NTT+EFOSC2 (resolution of 14 Å) and ∼22 Å for the VLT+FORS2 (resolution of 10 Å) at the position of Hα assuming a signal-to-noise ratio of greater than ∼20.

We have found for all the SN spectra in our sample that it is possible to distinguish between these two scenarios and so the roughly

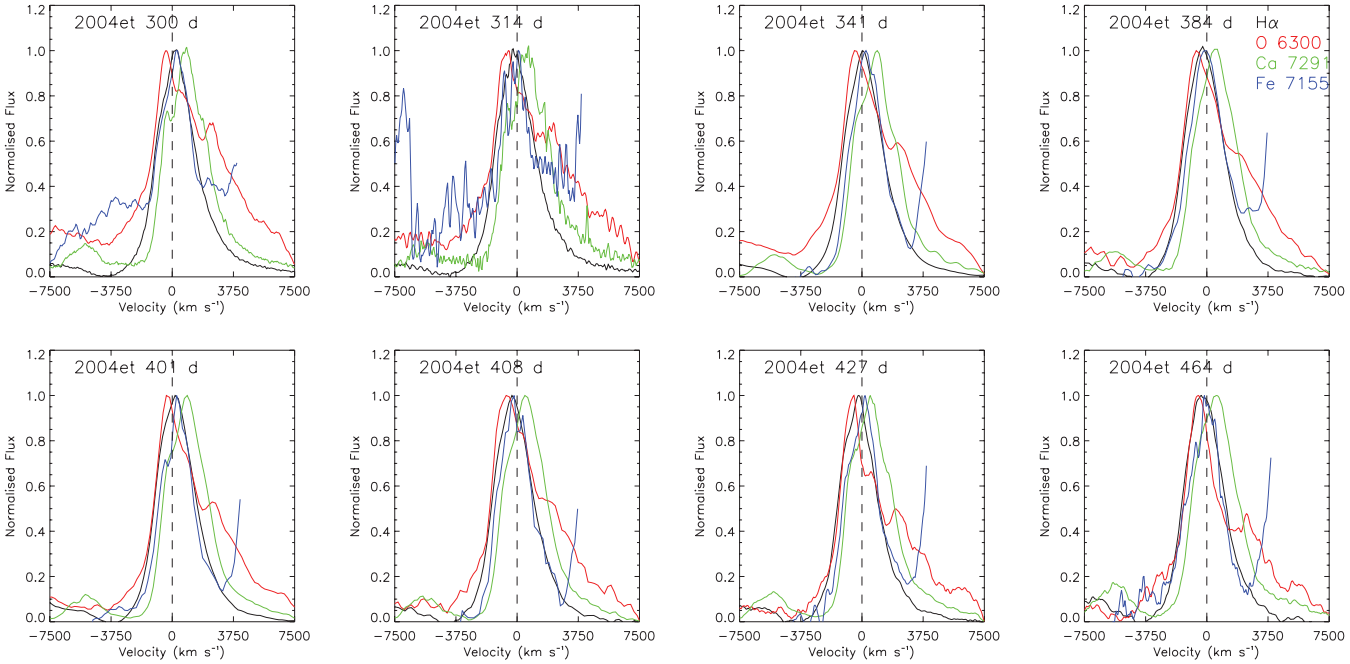

Figure 1. Line profiles for SN 2004et between 300 and 464 d. The [O I], [Ca II] and [Fe II] lines shown are doublets and have been centred on the blue component, as discussed in Section 4.1. The profile of Hα is shown in black, [O I] 6300, 6364 Å in red, [Ca II] 7291, 7323 Å in green and the [Fe II] 7155, 7172 Å doublet is shown in blue.

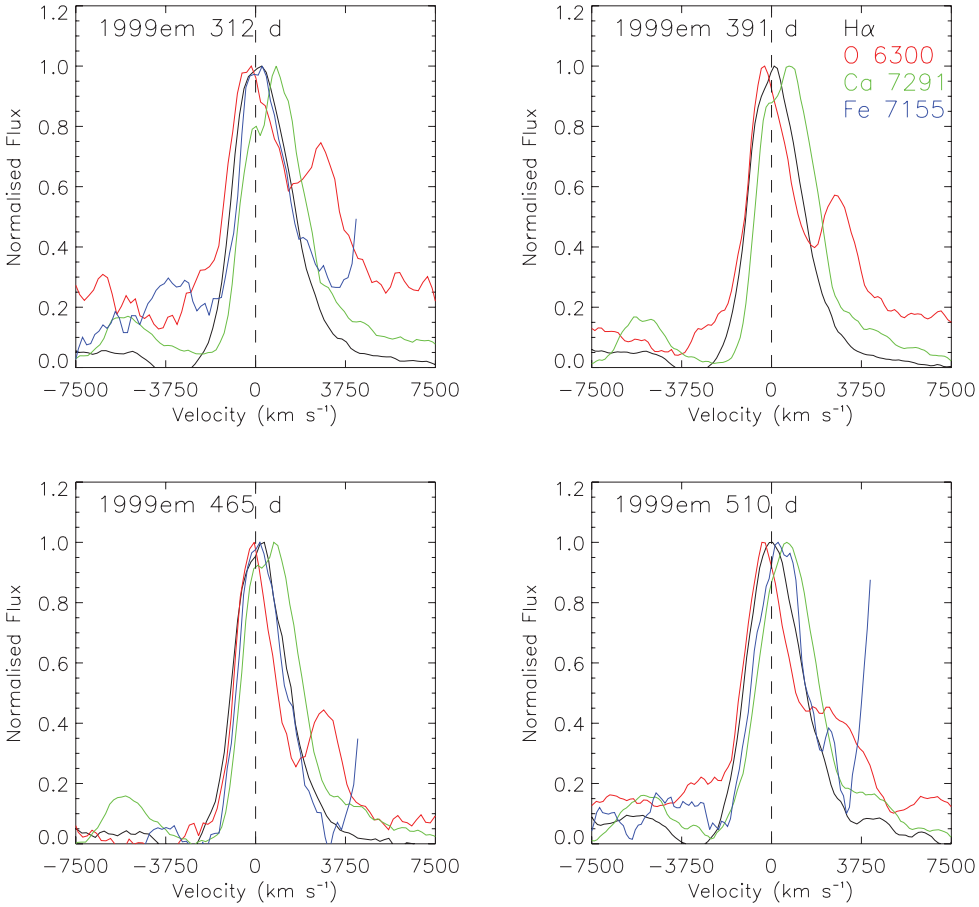

Figure 2. Line profiles for SN 1999em between 312 and 510 d. The lines are as specified in Fig. 1.

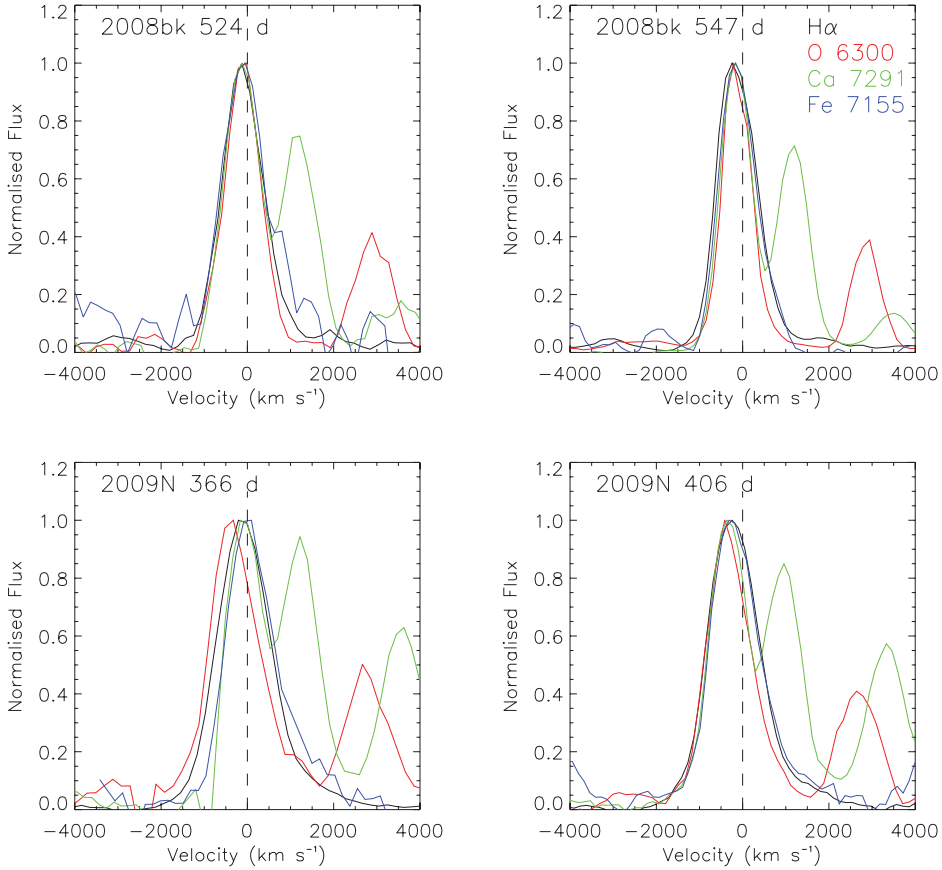

Figure 3. Line profiles for two low-luminosity SNe 2008bk and 2009N. The lines are as specified in Fig. 1.

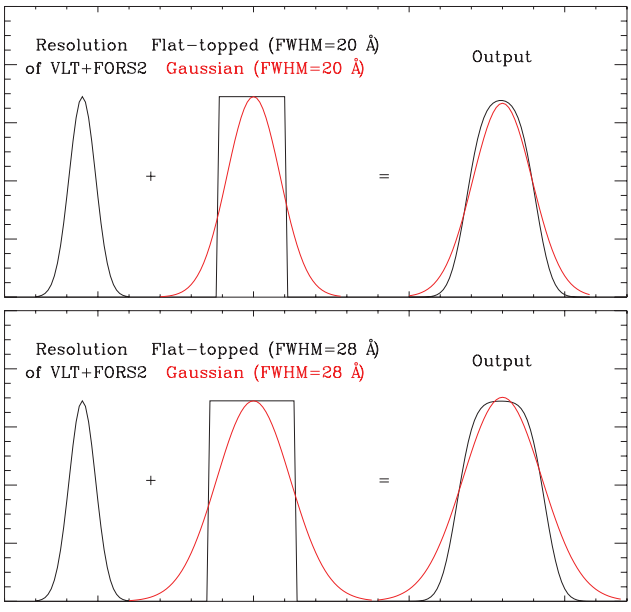

Figure 4. Comparison of the convolution of the instrumental resolution obtained with the VLT+FORS2 of 10 Å (measured from night sky lines) with both a flat-topped and a Gaussian profile. In the top panel, an $FWHM_{corr}$ of 20 Å is used, which corresponds to a post-convolution value of ∼22 Å, and it can be seen that the output line profiles are very similar and it is not possible to distinguish between them. In the bottom panel, an input $FWHM_{corr}$ of 28 Å is used, which corresponds to a post-convolution value of ∼30 Å, and the output line profiles for the flat-topped and Gaussian inputs are found to be different.

Gaussian-shaped profiles that are seen are found to be intrinsic to the SN emission, and this immediately suggests that mixing of the elements must occur in the SN ejecta to allow elements to be at zero velocity. Only for the spectrum of the narrow-lined SN 2008bk obtained at the NTT+EFOSC2 with a resolution of 14 Å, was it found to be not possible to distinguish between the intrinsic Gaussian profile and a flat-topped one. However, another spectrum of SN 2008bk was obtained at the VLT+FORS2 with a resolution of 10 Å, where it was possible to distinguish between these two scenarios and the line profile of Hα of SN 2008bk was found to be not intrinsically flat topped.

In Figs 1–3, it should be noted that the profiles of the different lines for a particular SN appear to have similar line profile shapes, which again suggests that the different elements producing the emission lines have a similar spatial distribution in the SN ejecta. In the early spectra of SN 2004et in Fig. 1 and for SN 1999em in Fig. 2, it appears as if the blue wing of the [O I] 6300 Å line extends to higher velocities than the other lines. However, this early blue wing of the [O I] 6300 Å line disappears at later times and is most likely caused by a blend with another emission line. In particular, Dessart, Livne & Waldman (2010) showed that there are many weak Fe lines in this region that could be blending with the [O I] doublet (see also Fransson & Kozma 2002). If the H emission lines were being produced solely in the envelope and the other elements from a central region, then it would be expected that the wings of the H profiles should extend to greater velocities, which does not appear to be the case. However, the velocities that can be measured from these emission lines are wavelength dependent and also must be corrected for the resolution of the instrument used to obtain the observations,

and therefore, a more quantitative analysis of this is presented in Section 4.2.

An evolution with time in the line profile shapes could be expected if at early times the emission mainly comes from regions close to the ^{56}Ni, but then as the gamma rays propagate outward, emission from other regions is seen. However, no evolution is seen with time, which could suggest that ^{56}Ni is not concentrated in the core of the SN but instead is distributed by mixing to regions farther out in the ejecta.

Asymmetry of some of the line profiles is seen in Figs 1–3. The nebular phase [O I] 6300, 6364 Å doublet of SN 2004et was investigated by Utrobin & Chugai (2009) for signs of possible asymmetry in the ejecta. They fitted three Gaussian components to each of the lines of the [O I] doublet and inferred a bipolar structure of the line-emitting gas in the inner layers of the SN envelope. They noted that this asymmetry refers to the line-emitting gas, which is not identical to the overall O distribution. An attenuation of the red wing (blueshift) of the line profiles of Hα and [O I] is seen for SN 2004et at ∼300 d and shown in Maguire et al. (2010) to be coeval with other indicators of dust formation. Dust condensation within the metal-rich ejecta of SN 1987A was first noted by Lucy et al. (1989) from the asymmetry of optical emission lines. Signatures of dust formation such as line attenuation were also seen for SN 1999em (Elmhamdi et al. 2003a) at ∼500 d post-explosion, and SN 2009N also appears to show a blueshifted profile for the [O I] 6300 Å line at both the epochs shown in Fig. 3, which is most likely due to dust formation in the ejecta.

Other signs of dust formation include a decrease in luminosity at optical wavelengths accompanied by an increase at near-infrared (NIR) wavelengths. Signatures of dust formation have been seen at mid-infrared wavelengths of IIP SNe to occur at similar epochs to the appearance of the blueshifted profiles for SNe 1987A (Meikle et al. 1993), 2003gd (Sugerman et al. 2006; Meikle et al. 2007), 2004dj (Meikle et al. 2011) and 2004et (Kotak et al. 2009). Therefore, the shapes of the emission lines along with other observational parameters tell us not only about the velocity distribution of the ejecta but also about the onset of dust formation and any possible asymmetric distribution of elements in the ejecta.

4.2 Velocity distribution

To study the distribution of elements in the ejecta and velocity at which the bulk of the emission occurs, the FWHM of the prominent emission lines in the sample of SNe were measured by fitting Gaussian profiles to each of the lines. The FWHM used were corrected as discussed in Section 4.1 for the resolution of the instrument used to obtain each spectrum using equation (1). From these corrected FWHM values, the half width at half-maximum (HWHM) velocities can be obtained to determine the velocity at which the different elements are found in the ejecta with respect to the zero velocity of the line profile.

The HWHM velocities of the sample of SNe studied here are shown in Fig. 5. The SN sample is split into three groups based on the average velocities of the emission lines. For the [O I] and [Ca II] doublets, the average value of the measurements of the two lines was used. Limits are shown for some of the emission lines when the individual components were not well enough resolved to fit Gaussians to each of the lines and were obtained by fitting a single Gaussian to the whole line profile. Therefore, these limits are very conservative upper limits for the widths of the individual lines. The outer wings of the line profiles could also be calculated from either the position at which the line flux goes to zero or the location of the first local minimum outward from the centre. The position of these outer wings would then tell us the velocity at which a certain element extends. However, the uncertainties in measuring these values are large due to the effects of blends of lines, contributions from the continuum and noisy spectra where the local minimum does not represent the true line minimum. Therefore, like Dessart et al. (2010), we have decided to use the more reliable HWHM for calculating the velocities, since it is more easily measured and compared among SNe.

Extensive studies of the emission line profiles of SN 1987A have been performed in the past, and as a consistency check, we have compared our measurements of SN 1987A to those of previous studies. Meikle et al. (1993) studied 1–4 μm spectroscopy of SN 1987A and found that the O I 1.129 μm velocities were lower than those of H, in agreement with Fig. 5. The [Fe II] and [Ca II] velocities of SN 1987A have only upper limits plotted, but the [Ca II] lines are consistent with having been produced in the inner regions of the H envelope as detailed in Li & McCray (1993a). The [O I] velocities are also consistent with those summarized in Li & McCray (1992). Li, McCray & Sunyaev (1993b) found that the Fe II, Co II and Ni II lines of SN 1987A have FWHM of 3000–3500 km s^{-1}, which are consistent with the HWHM velocity limits of [Fe II] shown here. The measurements of SN 1987A are consistent with those of previous studies, which suggests that our method of fitting the Gaussian profiles is sound.

In Fig. 5, there is a much larger difference between the Hα and [O I] velocity for SN 1987A than for the other SNe in the sample. This could suggest that the H envelope plays a role in contributing to the flux seen in the prominent emission lines for the other SNe, since the velocities for the different elements are relatively similar. The immediate physical interpretation of this is that a major fraction of the [O I] emission does not come from newly synthesized O, but from primordial O that is present in the H zones or from O clumps mixed to high velocities. For the low-luminosity, low-velocity events (SNe 2005cs, 2008bk and 2009N) shown in Fig. 5, actual measurements (instead of limits) of the expansion velocities were obtained for all the lines and it can be seen that Hα has higher velocities than the other lines, although the difference is not as great as in SN 1987A.

In Dessart et al. (2010), radiation-hydrodynamic simulations of IIP SNe were performed. They used a 1D model without mixing and suggested that their models of the chemical distribution of the ejecta in velocity space can be used to place strong constraints on the main-sequence masses of IIP SN progenitors. As shown above, the line profile shapes indicate that mixing is likely to have occurred in the ejecta of IIP SNe, and this argues against the assumption of chemical stratification in the SNe. While the Dessart et al. (2010) models are an informative first step in modelling nebular spectra to probe progenitor and explosion characteristics, the mixing of material in velocity space is likely an important parameter for future exploration. Dessart et al. (2010) used the width of the [O I] 6300, 6364 Å doublet to estimate the velocity of the O-rich zones as it was shown for SN 1987A at ∼500 d by Kozma & Fransson (1998a) that the [O I] lines were formed in the O-rich zones. However, in Section 5.1 we describe how a radiative transfer model can be used to determine the contribution to line emissions from different zones in the SN ejecta, and it is shown for a 12 $M_{\odot}$ model that the flux in the [O I] 6300, 6364 Å doublet has approximately equal contributions from primordial O in the H-rich zones and synthesized O in the

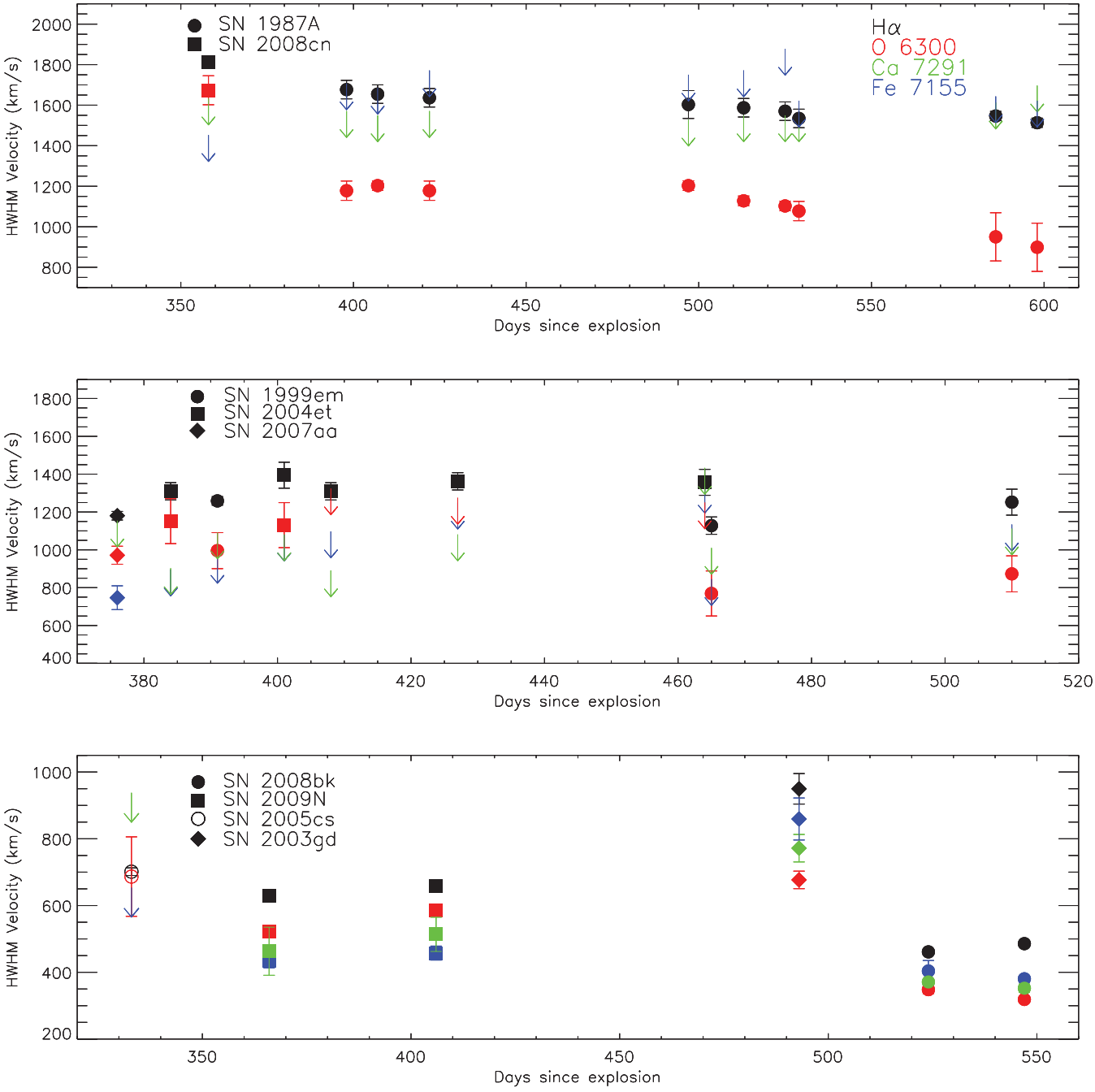

Figure 5. The HWHM (half the FWHM) velocities of the emission lines of Hα (black), [O I] (red), [Fe II] (blue) and [Ca II] (green) of SNe 1987A and 2008cn (top panel), SNe 1999em, 2004et and 2007aa (middle panel) and SNe 2008bk, 2009N, 2005cs and 2003gd (bottom panel) are shown. The SNe are grouped based on the average velocities of the emission lines. These velocities have been corrected for the intrinsic resolution of the instrument used to obtain each spectrum.

O-rich zones. However, as the mass of the progenitor increases, as in the case of SN 1987A, the contribution from the O core becomes dominant.

To investigate the effect of O emission from the envelope on the measured FWHM of the [O I] 6300, 6364 Å doublet, we used the spectrum resulting from the model detailed in Section 3. We compared the FWHM values obtained from the model spectrum with and without the contribution from the H zones and found that by excluding the contribution from the H zones, the FWHM of the [O I] 6300, 6364 Å doublet in the model spectrum was reduced by ∼8 Å, which corresponds to a HWHM velocity difference of ∼200 km s^{-1}. This would suggest that using the HWHM of the [O I] 6300, 6364 Å lines as an indicator of the extent of the spatial distribution of O would result in small but measurable overestimates of the velocities. The relatively small reduction of ∼8 Å when excluding the contribution from the H zones is due to the fact that while half of the [O I] flux is emitted by these zones, the main H zones contributing to the [O I] flux are those that are mixed into the core and therefore have a lower velocity than the average of all the H zones.

5 LINE FLUX ANALYSIS

5.1 Model results

The synthesized and primordial masses from our 12 $M_\odot$ model are given in Table 3 for some of the main elements, along with the ratio of primordial to synthesized mass for each of these elements. The primordial masses are those present in the H and He envelope at the end of the star's evolution. It can be seen that the synthesized masses are all larger than the primordial masses. However, when it comes to the observed spectrum it must be remembered that the flux in the emission lines will also depend on how efficient the element is at emitting per unit mass and how the energy is deposited in the ejecta.

The spectral synthesis model can be used to calculate the contributions to the luminosity of the prominent emission lines observed during the nebular phase from the various regions of the SN ejecta. In this section, we compare the output of the model to the observations in the range of 300–650 d. We make specific in-depth comparisons at 400 d, when most of the SNe in the sample have observed spectra. At this epoch, our model with a ^{56}Ni mass of 0.064 $M_\odot$ gives a total deposited energy of 1.9×10^{40} ergs, which is ∼75 per cent of the emitted energy (∼25 per cent of the gamma rays escape). The main characteristics of the model at 400 d are detailed in Table 4, including the energy deposited in each of the zones as well as the channels through which this deposited energy is released (heating of the gas, ionizations and excitations) and the main cooling lines. In this table, F_i is the fraction of the energy deposited into zone i, and $f^i_{\rm exc}$, $f^i_{\rm ion}$ and $f^i_{\rm heat}$ are the fractions of this energy going into non-thermal excitations, ionizations and heating, respectively. Finally, f^i_λ is the fraction of the cooling done by a given line in a given zone.

It can be seen that approximately 2/3 of the total energy is deposited in the H zones, with the next highest amount of deposited energy (∼1/6) going into the He zone. Since most of the energy is deposited in the H zones and mainly released by heating of the gas, it is expected that nebular phase spectra should be dominated by thermal line emission from H-rich material. The main cooling lines in the H zones during the first year are lines at UV wavelengths such as the Mg II 2795, 2802 Å and Fe II 2382, 2600 Å lines. However, there is also an appreciable contribution from cooling lines in the optical that can be analysed. Although the He zone gets ∼1/6 of the energy, it does not produce any distinct optical lines that can be studied. For most of the zones at 400 d, it can be seen that heating is the dominant channel for the deposited energy, with ionization the next most important, while only a small percentage of energy goes into excitations.

The excitation of the lines can in general be divided into those excited thermally and those excited by recombinations. The recombination lines arise as a result of the non-thermal ionizations and in some cases, like H, photoionizations. They are therefore insensitive to the temperature and mainly depend on the efficiencies for ionization by the gamma rays and the ionizing UV radiation. The thermally excited lines are responsible for most of the cooling of the ejecta. The strength of a given line from a specific abundance zone is determined by the fraction of energy deposited in that zone and the relative abundances in this zone. However, the efficiencies of different elements in cooling are very different, depending on their atomic structure. As an example the [Ca II] 7291, 7323 Å lines are typically 10^2–10^3 times more efficient per atom in cooling than the [O I] 6300, 6364 Å lines. A small abundance of Ca can therefore dominate that of the much more abundant O (Fransson & Chevalier 1989). The luminosity, $L(\lambda)$, of the different lines can be estimated from Table 4 using

$$L(\lambda) = E_{\rm tot} F_i f^i_{\rm heat} f^i_\lambda, \quad (2)$$

where $E_{\rm tot}$ is the total energy deposition (in the whole ejecta) and the other quantities are defined above and in Table 4. We discuss the individual lines here, referring specifically to the model described above.

Table 3. Primordial and synthesized masses of the listed elements from the 12 $M_\odot$ model used in this paper, along with the ratio of primordial to synthesized mass for each of the elements. The Fe mass is calculated at 400 d for a ^{56}Ni mass of 0.064 $M_\odot$.

Element	Synthesized mass ($M_\odot$)	Primordial mass ($M_\odot$)	Synthesized/primordial mass ratio
O	3.08×10^{-1}	4.45×10^{-2}	6.9
Si	4.12×10^{-2}	7.12×10^{-3}	5.8
S	2.63×10^{-2}	3.65×10^{-3}	7.2
Ca	2.40×10^{-3}	6.41×10^{-4}	3.7
Fe	6.5×10^{-2}	1.22×10^{-2}	5.4

Table 4. Output values for the model at 400 d: total energy deposition, energy channels and dominant cooling lines for each zone.

Zone	Fe/He	Si/S	O/Si/S[b]	O/Ne/Mg	O/C[b]	He[a]	H[a]
Energy deposition per cent ($F_{\rm zone}$)	7.5	1.9	2.5	2.5	2.9	16.2	67
Breakdown of energy channels							
Heating per cent[a] ($f^{\rm zone}_{\rm heat}$)	76	52	43	52	43	43	35
Ionization per cent ($f^{\rm zone}_{\rm ion}$)	18	29	47	42	49	44	37
Excitation per cent ($f^{\rm zone}_{\rm exc}$)	6	19	10	6	8	13	28
Breakdown of cooling lines							
[Ca II] (7291, 7323 Å) ($f^{\rm zone}_{7291}$)	2.4	47	0	7.2	0	2.3	27
[O I] (6300, 6364 Å) ($f^{\rm zone}_{6300}$)	0	0	0	55	0	0	4.4
[Fe II] (7155, 7172 Å) ($f^{\rm zone}_{7155}$)	7.4	0.6	0	0.3	0	0.3	1.7

[a]Energy deposition channels are calculated for the H and He zones using a mean, weighted by the energy deposition in each zone.
[b]The zero values are due to molecule formation, which we assume is responsible for the cooling in these zones.

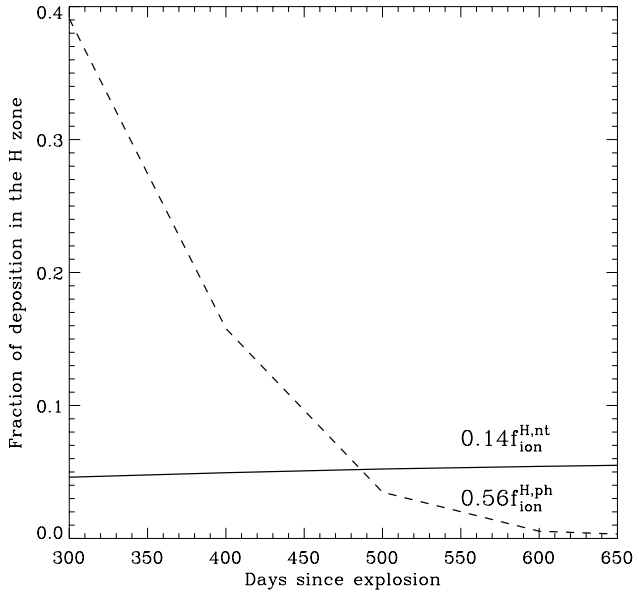

Figure 6. The contribution to the Hα luminosity from non-thermal ionizations, $f_{\rm ion}^{\rm H,nt}$ (solid line), and from photoionizations, $f_{\rm ion}^{\rm H,ph}$ (dashed line).

5.1.1 Hα

Hα is not an efficient cooler because the $n = 3$ state has too high an excitation energy (10.2 eV) and Hα is instead created by recombinations, and to a lesser extent by non-thermal excitations. The importance of photoionizations from the $n = 2$ state by UV photons was first shown by Kirshner & Kwan (1975). The model results for the relative contributions are shown in Fig. 6 and found to be in good agreement with the results of Xu et al. (1992). $f_{\rm ion}^{\rm H,nt}$ is the fraction of the energy deposited in the H zones going into non-thermal ionizations and $f_{\rm ion}^{\rm H,ph}$ is the fraction of the energy deposited in the H zones going into Balmer photoionizations. The value 0.14 is the fraction of non-thermal ionization energy re-emitted as Hα (1.89 eV/13.6 eV) and 0.56 is the fraction of Balmer photoionization energy re-emitted as Hα (1.89 eV/3.4 eV), where 1.89 eV is the energy of the Hα photon and 3.4 eV is the ionization potential of the Balmer continuum. Using our calculation, which includes a detailed computation of the internal UV field, we confirm the results in Xu et al. (1992) and Kozma & Fransson (1992), that Balmer photoionizations are dominant in the H ionization rates up to ∼400–500 d. At this time a transition to the non-thermal dominated phase occurs, when the Balmer continuum becomes optically thin and direct ionizations from non-thermal electrons dominate. At 400 d, we find a deposition-weighted ratio of Balmer to non-thermal ionization of ∼3 (see Fig. 6).

5.1.2 [O I] 6300, 6364 Å

The emission in the [O I] 6300, 6364 Å lines is caused by a combination of emission from synthesized and primordial O. There are three zones that contain O as their main component: O/Si/S, O/Ne/Mg and O/C. In the O/Si/S and O/C zones, modelling has shown that molecules of SiO and CO form and are responsible for nearly all of the cooling (Liu & Dalgarno 1995). This is supported by the detection of SiO and CO in SN 1987A (Aitken et al. 1988; Spyromilio et al. 1988), as well as in other IIP SNe such as SN 2004et (Kotak et al. 2009; Maguire et al. 2010). Therefore, we can expect to see thermal emission from synthesized O from the O/Ne/Mg zone only. In this zone, the [O I] 6300, 6364 Å doublet is one of the dominant cooling lines doing about half of the total cooling and provides a significant contribution to the [O I] 6300, 6364 Å line luminosity.

However, there is also a contribution to the [O I] doublet from primordial O in the H zones, where the doublet is found to do a few per cent of the total cooling. From Table 4 the fraction of the total emission in the [O I] lines from the O/Ne/Mg zone is $\sim 0.025 \times 0.52 \times 0.55 \approx 0.0072$, while it is $\sim 0.67 \times 0.35 \times 0.044 \approx 0.010$ in the H envelope. The low fraction of the cooling done by the [O I] lines in the H envelope is therefore balanced by the large total energy deposition in this zone.

This leads to the important conclusion that in IIP SNe with progenitor masses of $\sim 12\,{\rm M}_{\odot}$, the [O I] emission is formed by approximately equal contributions from primordial and synthesized O. This is perhaps surprising since approximately six times more synthesized O than primordial O is present (assuming solar metallicity), but this is negated by the fact that the H zones absorb approximately eight times more gamma-ray energy than the O zones, and also that the O/Si/S and O/C zones are cooled by molecules.

This is different to the results that were obtained for SN 1987A using a $20\,{\rm M}_{\odot}$ model, where it was found that [O I] emission lines are formed in the zones containing synthesized O (Kozma & Fransson 1998a). Woosley & Weaver (1995) showed that the O mass depends sensitively on the progenitor mass; a $20\,{\rm M}_{\odot}$ main-sequence star would produce an O mass of $1.8\,{\rm M}_{\odot}$ and the synthesized O mass would be ∼40 times greater than the primordial O mass, and so the contribution of synthesized O to the total [O I] 6300, 6364 Å lines should dominate. These models for SN 1987A also assumed a lower amount of O in the envelope due to CNO mixing than obtained in the stellar evolution models used here.

5.1.3 [Ca II] 7291, 7323 Å

Synthesized Ca exists mainly in the Si/S zone ($2.1 \times 10^{-3}\,{\rm M}_{\odot}$), but also in the Fe/He zone ($3.2 \times 10^{-4}\,{\rm M}_{\odot}$), while the total mass of primordial Ca present in the envelope is $6.4 \times 10^{-4}\,{\rm M}_{\odot}$ (∼25 per cent of the synthesized mass). As was previously shown by Li & McCray (1993a) and Kozma & Fransson (1998a) for SN 1987A, it is found for our $12\,{\rm M}_{\odot}$ model that the [Ca II] 7291, 7323 Å doublet is formed nearly completely by primordial Ca in the inner regions of the H envelope. The [Ca II] 7291, 7323 Å emission from the Si/S and Fe/He zones is no more than ∼10 per cent of the total flux at any time. This is because the masses of these zones are small compared to the H zones and so receive only a small amount of gamma-ray energy. At later times, the [Ca II] lines will receive important contributions from fluorescence (Li & McCray 1993a) but at ∼400 d the [Ca II] emission from the H envelope is dominantly thermal.

5.1.4 [Fe II] 7155, 7172 Å

The [Fe II] 7155, 7172 Å doublet has a flux ratio of its components of ∼3 to 1 if the parent multiplet is in local thermodynamic equilibrium and optically thin. The state from which the doublet comes is only 1.95 eV above the ground state, so this transition is thermally driven. The [Fe II] 7155, 7172 Å doublet is formed by contributions from both synthesized Fe from the Fe/He zone and primordial Fe in the H envelope. From Table 4, one finds from the products of the energy deposition, heating fraction and cooling fraction that there are equal contributions from the Fe/He zone and the H envelope to this line. This line, like the [O I] and [Ca II] doublets, is therefore a mix of synthesized and primordial Fe, which is in agreement with the results for SN 1987A (e.g. Kozma & Fransson 1998a).

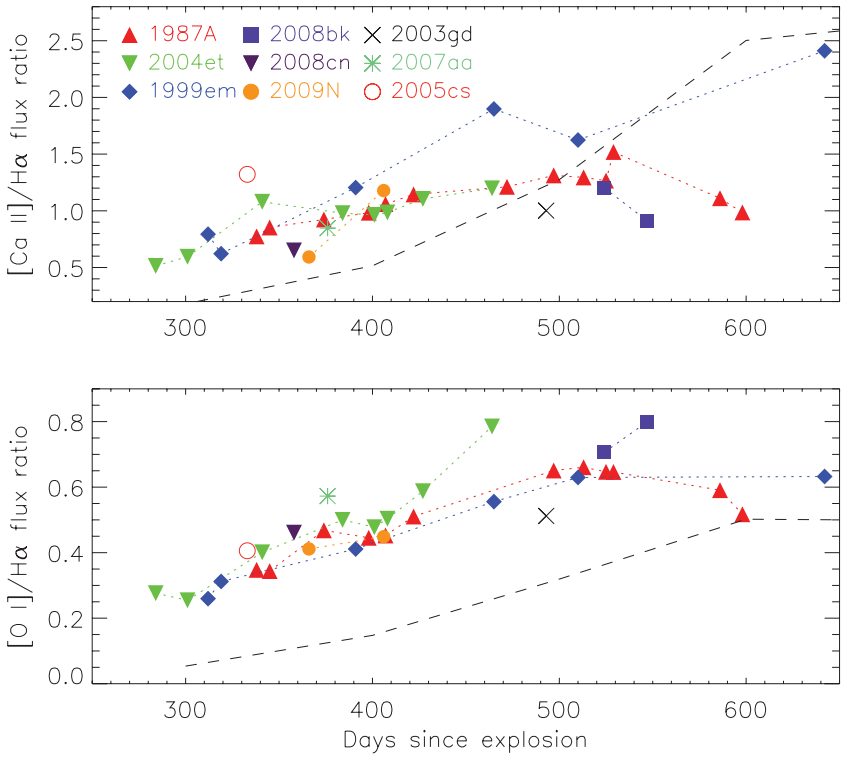

Figure 7. From top to bottom, the ratio of the flux in the [Ca II] doublet to Hα and the ratio of the [O I] doublet to Hα. The dashed black line shows the output from the model.

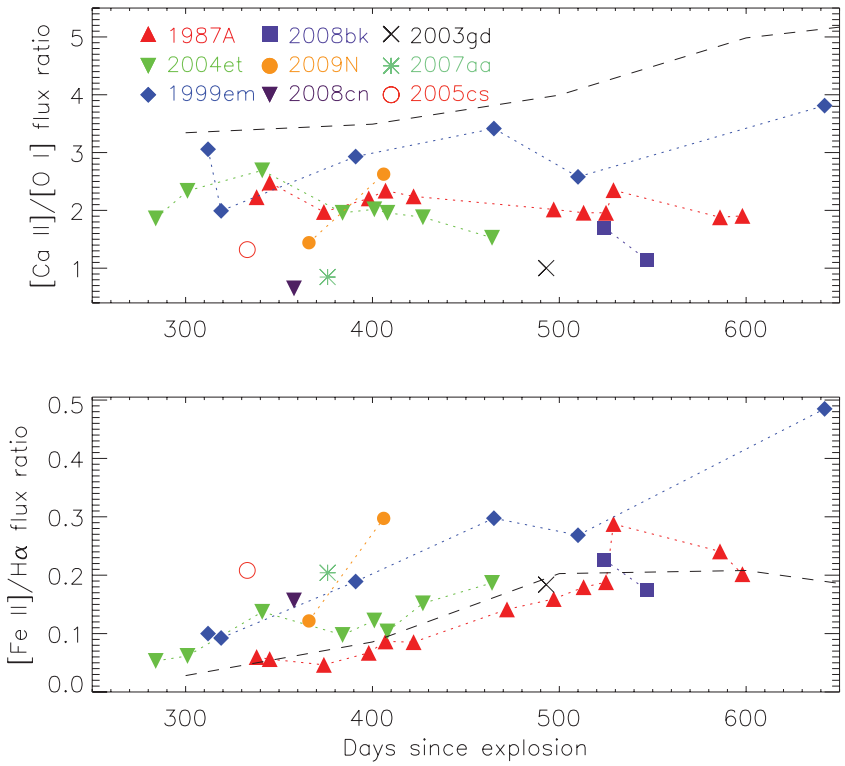

Figure 8. Ratio of flux in [Ca II] to [O I] and ratio of flux in [Fe II] to Hα. The dashed black line shows the output from the model.

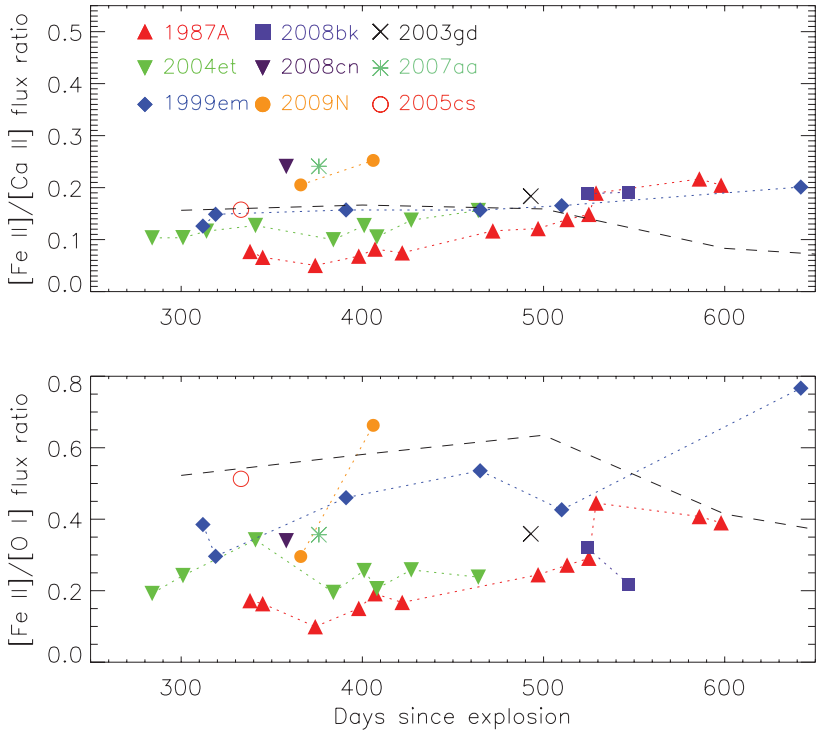

Figure 9. Ratio of flux in [Fe II] to [Ca II] and [O I]. The dashed black line shows the output from the model.

5.2 Application to observed line flux ratios

Having obtained a theoretical interpretation of the origin of the flux in the prominent emission lines and the dominant processes involved (ionization in the case of Hα and heating for the rest of the studied lines), these results can then be compared to the values obtained from our late-time nebular phase spectra using flux ratios of the prominent emission lines. Line ratios are a convenient method of comparing emission line properties of SNe both as a function of time and between different objects, because any uncertainty in calibrating the absolute flux of the spectra is removed.

The line ratios were measured by fitting a Gaussian to the line profiles and then integrating the flux under the curve and subtracting off a linear continuum. In the case of the doublets of [O I], [Ca II] and [Fe II] where the individual component lines were blended, both lines were fitted simultaneously with two Gaussians to obtain the total flux. In Figs 7–9, the ratios of the prominent emission lines (Hα, [O I] 6300, 6364 Å, [Ca II] 7291, 7323 Å and [Fe II] 7155, 7172 Å) for the nine SNe described in Section 2 are shown, along with the model curve obtained from the spectral synthesis model detailed above. The flux ratios outputted from the model are for a 12 $M_{\odot}$ model with a core velocity of $\sim$1800 km s^{-1}. As noted in Section 3, this model is not suitable for calculating line flux ratios of low-luminosity, low-velocity events such as SN 2008bk (core velocity of $\sim$600 km s^{-1}) due to strong adiabatic cooling at these velocities, which makes steady-state temperature calculations unreliable. Therefore, comparisons of low-velocity events such as SNe 2008bk and 2009N with the model output in Figs 7–9 should be treated with caution.

First, it can be seen in Figs 7 and 8 that there is a trend of increasing flux from the [Ca II], [O I] and [Fe II] lines with time compared to Hα. This can be understood based on the transition, as detailed in Section 5.1.1, of the Balmer continuum to an optically thin regime and is shown in Fig. 6. The contribution of the Balmer

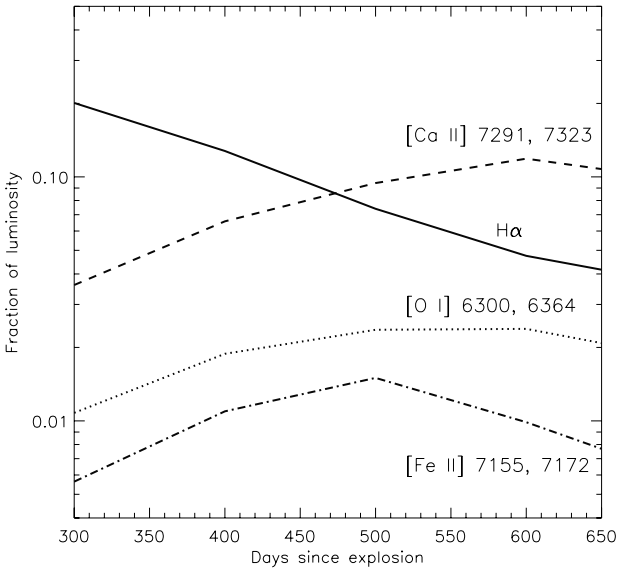

Figure 10. The fraction of the total luminosity emerging in Hα (solid line), [O I] 6300, 6364 Å (dotted line), [Ca II] 7291, 7323 Å (dashed line) and [Fe II] 7155, 7172 Å (dash-dot line) in the spectral synthesis model.

continuum photoionization to the total ionization rate decreases with time, and hence, the Hα luminosity also decreases. Also, we see in Fig. 10 that the fraction of the total luminosity that is carried by the optical cooling lines increases up to 500–600 d, as the temperature falls to favour optical over UV line cooling. At $\sim$600 d, infrared lines take over and the optical lines decrease.

The [Ca II] 7291, 7323 Å to Hα model ratio as a function of time is plotted in Fig. 7 and found to be slightly lower at early times, but is in reasonable agreement with the observed flux ratios. The [Ca II] to Hα ratio displays little variation between the different SNe

and this can be understood by both of the lines being formed in the H zones, and therefore is independent of their synthesized masses, and the relative amounts of energy going into heating (responsible for the [Ca II] emission), and ionization (responsible for the Hα emission) are not very sensitive to the density and temperature.

The [O I] 6300, 6364 Å to Hα model ratio shows the same trend as the observed flux but is lower at all epochs. Since this is the same underproduction trend as seen at earlier times for the [Ca II] to Hα ratio, Hα may be overproduced in the model. The scatter in the ratio between different SNe does not seem to show any trend with ^{56}Ni or progenitor mass. Although the synthesized O to H ratio should grow with progenitor mass, the significant contribution from primordial O will damp the impact of this on the [O I] 6300, 6364 lines. It is surprising that SN 1987A does not have the highest value since its [O I] emission was shown (Kozma & Fransson 1998a) to be dominated by emission from the O-rich zones, which should be significantly greater in a 20 $M_\odot$ star compared to a low mass star. This suggests that either the mass of synthesized O is smaller than previously believed, or that SN 1987A is unusually H-rich.

The [Ca II] to [O I] ratio is also shown in Fig. 8 and suggests that either [Ca II] is being overproduced in the model or [O I] underproduced. A wide range of observed values are seen for this ratio, but there is no very noticeable trend with SN properties. There may be a weaker [Ca II] to [O I] flux ratio for lower velocity SNe such as SNe 2008bk and 2003gd seen at ∼500–550 d compared with the model, which could be explained by [Ca II] emission doing less cooling in the H zones at the lower temperatures (of the order of 1000 K) seen in low ^{56}Ni mass events (Jerkstrand et al., in preparation), but synthesized [O I] still doing most of the cooling in the O zones due to fewer competing cooling lines. However, this is a speculative explanation and the high-velocity SN 2008cn and 'normal' velocity SN 2007aa also show weak [Ca II] to [O I] ratios at ∼350 d which cannot obviously be explained in this way. Further modelling using a variety of velocity and ^{56}Ni mass inputs will be used to explore this in more detail.

The other prominent emission line studied here is the [Fe II] 7155, 7172 Å doublet, which is detailed in Section 5.1.4. The ratio of [Fe II] to Hα model curve is shown in Fig. 8, which is in good agreement with the observed range. There is a trend of increasing flux with time of [Fe II] with respect to Hα, but no obvious trend between SNe with different ^{56}Ni masses and velocities is seen. The ratio of the [Fe II] 7155, 7172 Å doublet to the [Ca II] 7291, 7323 Å line is plotted in Fig. 9, and again good agreement between the model and observed ratios is seen. The [Fe II] to [Ca II] ratio seems to be relatively constant as a function of time and no obvious trend with ^{56}Ni mass or velocity can be observed. The ratio of the [Fe II] 7155, 7172 Å doublet to the [O I] 6300, 6364 Å doublet can be obtained using combinations of the primordial and synthesized O and Fe components, and is shown in Fig. 9. The scatter in the observed values for the different SNe is quite large compared to the [Fe II] to [Ca II] ratio shown above, perhaps due to varying contributions from synthesized O to the [O I] lines.

This is the first time that the nebular phase spectra of IIP SNe have been compared in detail and interpreted in the framework of a radiative transfer model. SN1987A has been the cornerstone of understanding synthesized material ejected in SNe in relation to a progenitor of known mass, but we now have a sample of SNe with progenitor constraints and good quality nebular phase spectral coverage. No significant trends with progenitor mass are seen, with all the SNe in the sample having very similar flux ratios for the different elements. This suggests that we are, in general, seeing emission from similar regions for the different SNe in the sample.

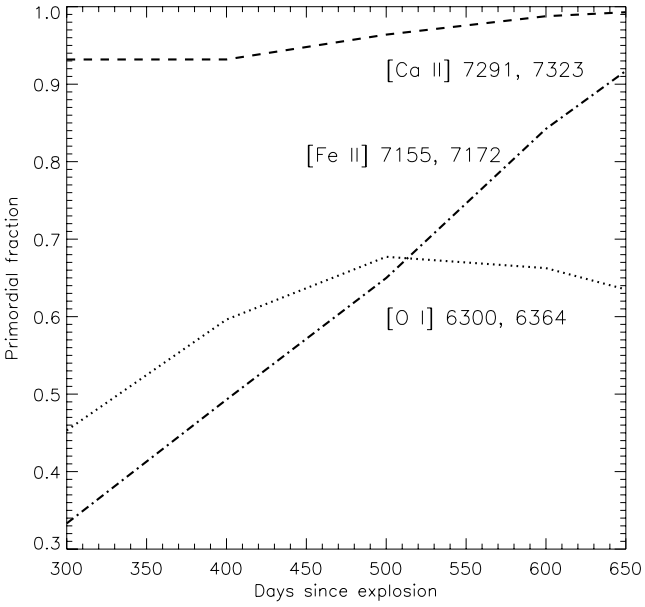

Figure 11. Fraction of [O I] 6300, 6364 Å (dotted line), [Ca II] 7291, 7323 Å (dashed line) and [Fe II] 7155, 7172 Å (dash-dot line) lines being produced by primordial abundances in the H zones relative to their total flux as a function of time since explosion.

The observed line widths and line profiles, along with the theoretical interpretation of the line ratios, suggest like for SN 1987A (Kozma & Fransson 1998a; Li & McCray 1993a; Li et al. 1993b) that [Ca II] emission is formed in the H zones and the [Fe II] emission is produced by a mixture of primordial and synthesized Fe.

However, the most important result discovered here using the line profiles and widths and also the theoretical interpretation is that for our 12 $M_\odot$ model, the [O I] 6300, 6364 Å emission lines are formed from nearly equal contributions from primordial O in the H-rich zones and synthesized O in the O-rich zones. Fig. 11 shows a plot of the relative contribution from primordial abundances as a function of time for the [O I], [Ca II] and [Fe II] lines. At earlier times, the [Ca II] lines are mainly formed from thermal processes, while at later times, there is also a contribution from fluorescence. Both thermal emission and fluorescence occur mainly in the H zone at all times. For the [O I] doublet, the division between synthesized and primordial material is ∼50 per cent each at all times. With time, the [Fe II] 7155, 7172 Å doublet becomes steadily more dominated by the H zone, as the Fe/He zone rapidly cools to temperatures where infrared cooling dominates (Kozma & Fransson 1998b). This is markedly different to the results obtained for SN 1987A, which showed that the emission was being produced nearly completely in the O-rich zones (Spyromilio & Pinto 1991; Li & McCray 1992; Kozma & Fransson 1998a). The reason for this is twofold; the mass of synthesized O is ∼10 times larger in a 20 $M_\odot$ star compared to a 12 $M_\odot$ star, and the abundance of O in the envelope of SN 1987A was found to be strongly suppressed by CNO mixing.

5.3 Implications for synthesized O mass estimates

In the past, the [O I] 6300, 6364 Å flux has been used to estimate the mass of synthesized O and hence the main-sequence mass of the progenitor star. Elmhamdi et al. (2003a) used an equation that calculated the O mass in SN 1999em by using a ratio with SN 1987A involving its O luminosity in the [O I] 6300, 6364 Å lines and its ^{56}Ni mass during the tail phase. Uomoto (1986) estimated

the minimum mass of O needed to produce the [O I] emission lines during the nebular phase, using an equation that depended on the flux of the [O I] lines, the distance to the SN and the temperature of the emitting gas. The O mass of SN 1987A has been modelled in detail and found to be in the range 1.2–1.5 $M_{\odot}$ (Kozma & Fransson 1998a; Chugai 1994).

However, unlike SN 1987A, the IIP SNe studied here result from the collapse of significantly less massive stars and we see evidence that the [O I] emission is made up of contributions from primordial and synthesized O, and so the [O I] doublet is not a simple, direct indicator of the synthesized O mass. Therefore, the O mass estimates in the literature for IIP SNe with low progenitor mass estimates should be treated with caution (e.g. Elmhamdi et al. 2003a; Pozzo et al. 2006; Maguire et al. 2010; Andrews et al. 2011; Elmhamdi 2011), since they are based on an analysis of SN 1987A, and the true O masses could be only ∼50 per cent of these values. However, the O mass can still be estimated as long as the flux contribution from primordial O in the H zones is subtracted off first. An updated estimate of the synthesized O mass of SN 2004et is determined in Jerkstrand et al. (in preparation) and can be used in the future for comparisons with SNe with low mass progenitor estimates.

5.4 [O I] 6300, 6364 Å line ratio

The ratio of the 6364 Å to the 6300 Å line in the [O I] doublet can be used to determine whether the O-emitting zones are optically thick or optically thin (Spyromilio & Pinto 1991; Li & McCray 1992). In Fig. 12, the ratio of the 6364 Å to the 6300 Å line is shown for a sample of eight IIP SNe. In the optically thick limit, the ratio of their intensities is 1:1, while in the thin limit the ratio of the intensities of the lines should be 1:3. An evolution from optically thick towards optically thin is seen for the sample of SNe in Fig. 12. The theoretical curve for an O number density of 7×10^{10} cm^{-3} at 100 d is also plotted in Fig. 12.

A contribution of up to ∼20 per cent from the Fe I 6361 Å line to the flux in the [O I] 6364 Å line was found for SN 1987A by Kozma & Fransson (1998a). This was investigated for this model, but at 400 d, the Fe I 6361 Å line was found to be a less than 3 per cent contaminant and no other lines were found in this wavelength region. Instead, we find that opacity due to other lines may influence the [O I] line ratio. The escape probability for photons with respect to absorption in other lines is dependent on wavelength. For the two [O I] 6300, 6364 Å lines there is an ∼60 per cent and ∼75 per cent chance of escaping, respectively. This will increase the 6364/6300 ratio, since the 6364 Å photons will escape somewhat more easily (by a factor of 1.25 in this case).

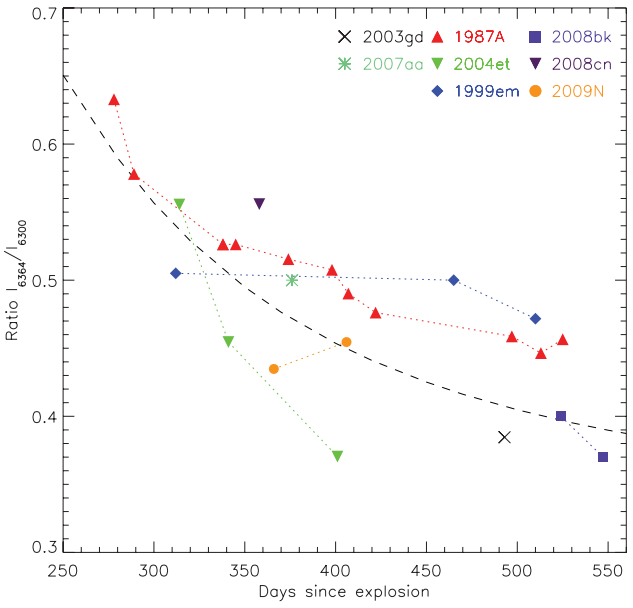

Figure 12. Ratio of the flux in the [O I] 6364 Å to the 6300 Å lines. The black dashed line is the theoretical curve for an O number density of 7×10^{10} cm^{-3} at 100 d.

There is a significant difference in the rate at which the O-emitting regions become optically thin for different SNe. SN 2004et shows a steep decline towards the optically thin regime, which might suggest that the density of its ejecta is low, which can be explained by the high HWHM [O I] velocities seen for SN 2004et of ∼1200 km s^{-1} during the nebular phases studied. In a similar way, the low-velocity SN 2008bk had lower HWHM [O I] velocities (∼350 km s^{-1}) and therefore remained denser for longer and hence took longer for its ejecta to become optically thin. However, SN 1987A, like SN 2004et, had high [O I] velocities (∼1100 km s^{-1}) and therefore should have become optically thin at a similar rate to SN 2004et, but this evolution is not seen. This could be due to the large contribution from the synthesized [O I] in the core, where the densities are higher.

Indeed, this ratio can be used to probe the density structure of the O-emitting regions as was done for SN 1987A by Li & McCray (1992) and Spyromilio & Pinto (1991). However, unlike SN 1987A, it has been shown for lower mass stars that the [O I] 6300, 6364 Å doublet is formed equally by contributions from the envelope and O-rich zones, and so any density estimates must use a two-component model to fit the contributions from both the H-rich and O-rich zones.

6 LINE IDENTIFICATIONS OF SN 2008BK

A late-time nebular spectrum (+547 d) of SN 2008bk is shown in Fig. 13, along with a model spectrum outputted from the spectral synthesis code. The identifications do not distinguish between forbidden and allowed lines; instead it identifies which element contributes most to which features. This SN has very low line velocities that give narrow emission lines that are well resolved. In higher velocity events, such as SN 2004et, many lines are blended not due to the resolution limit of the instruments used to obtain the spectra but because their profiles intrinsically overlap in velocity space. Therefore, low-velocity SNe give us a great opportunity to identify individual line emissions that would be blended in higher velocity events. The prominent emission lines in this spectrum were identified using the same spectral synthesis code as discussed earlier, again using a 12 $M_{\odot}$ model, but this time choosing a core velocity of 600 km s^{-1} to match the velocities seen in SN 2008bk. Adiabatic is strong relative to line cooling in the envelope, as the low ^{56}Ni mass implies a low electron fraction and low collision frequencies. This makes the steady-state temperature calculation unreliable, and therefore, this model has not been used to calculate flux ratios. However, the line identifications should not be affected and can be used to identify the spectral features in low-velocity spectra such as those of SN 2008bk.

Most of the lines in the complex region from 4000 to 5500 Å can be identified with the [Fe I] and [Fe II] lines, created by scattering and fluorescence in the H envelope. Above 5500 Å the core zones start making contributions to the spectrum. The 5900 Å line is Na I 5896 Å which scatters emission from the Na I 5890 Å line, as well

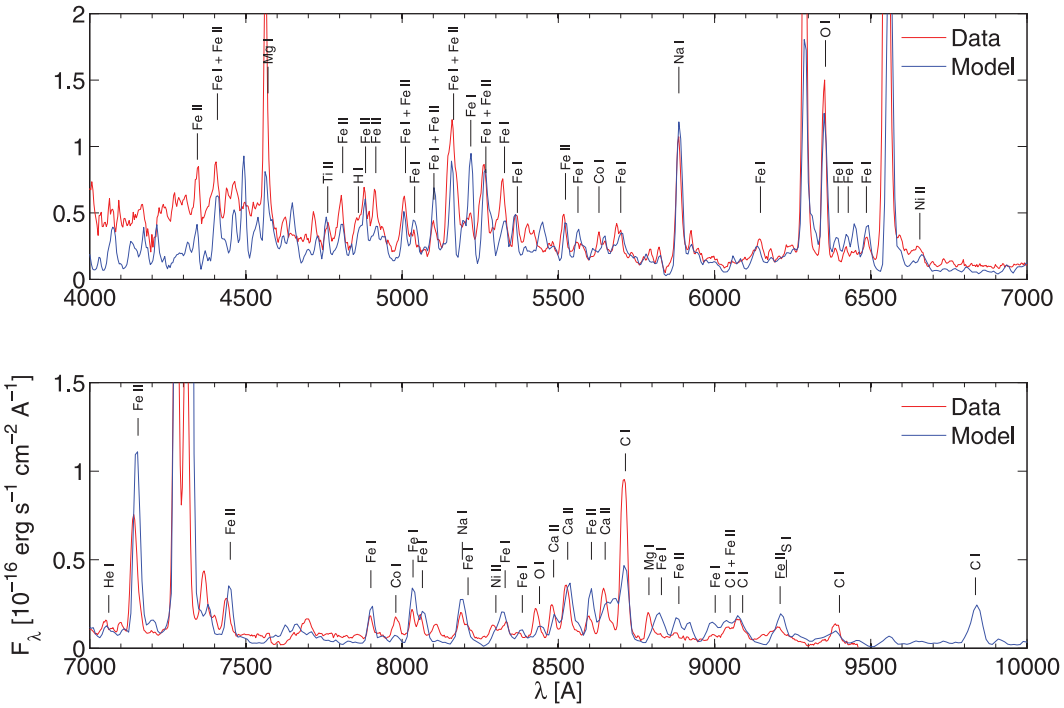

Figure 13. Line identification for the low-velocity SN 2008bk at +547 d post-explosion comparing the spectral synthesis model (blue) to the data (red). We have not distinguished between forbidden and allowed lines; instead we show which ion contributes most to which feature.

as from the He I 5876 Å line, with about a third of the photons emitted by synthesized Na in the O/Ne/Mg zone. The Fe I lines at 7900, 8030, 8060, 8200, 8300 and 8350 Å are all from Fe in the core (both from the Fe/He clumps and from the O/Ne/Mg clumps). In the NIR, we can identify the O I 8446 Å line, which is usually hard to see due to blending with the Ca II triplet in higher velocity SNe. Another line which usually also suffers from this blending is [C I] 8727 Å which is clearly seen here. In the model, this line, along with the C I lines at 9000–9100 Å and 9400 Å, is created by C in the He envelope, verifying that significant dredge-up has occurred in this star.

7 CORRELATION OF VELOCITY WITH ^{56}Ni MASS

There are currently a number of methods by which the ^{56}Ni mass ejected in a IIP SN can be estimated. Most methods require knowledge of the bolometric light curve of the SN during the early radioactive tail phase. During this phase, the bolometric light curve is powered nearly completely by the radioactive decay of ^{56}Co to ^{56}Fe, and hence the luminosity at this stage gives a good indication of the synthesized ^{56}Ni mass that is ejected in the explosion. The link between the light curve and ^{56}Ni mass can be made in three different ways: a comparison with the luminosity of SN 1987A, which has a well-constrained ^{56}Ni mass, the steepness parameter method of Elmhamdi, Chugai & Danziger (2003b) and the tail luminosity method of Hamuy (2003). However, the use of these methods is limited to SNe with good bolometric coverage during the radioactive tail phase, as well as reliable distance and extinction estimates.

For SNe with limited multiband coverage, Bersten & Hamuy (2009) and Maguire et al. (2010) described bolometric corrections to convert from a magnitude obtained in a single band to a bolometric luminosity. The former paper estimated the correction as a function of colour, while the latter work as a function of time since explosion. These corrections are useful for sparsely covered events, but still require an accurate estimate of the extinction and distance to the SN. Using late-time spectra (200–400 d post-explosion), Chugai (1990) and Elmhamdi et al. (2003b) described how the luminosity of the Hα emission line is proportional to the ejected ^{56}Ni mass. This method is useful when no photometry is available, but again the distance and extinction to the SN must be known. Therefore, independent methods that do not rely on knowledge of the absolute magnitude of the SN would be a useful addition. Hamuy (2003) showed a correlation between the ^{56}Ni mass and the photospheric velocity at mid-plateau. However, the photospheric velocity decreases rapidly during the photospheric phase and therefore requires a well-sampled light curve to provide a secure constraint on the explosion epoch to obtain the velocity mid-plateau. In this section, we discuss a method for estimating the ejected ^{56}Ni mass from the FWHM of the emission lines observed in the nebular phase spectra of IIP SNe, where the velocity is found to be relatively constant in the range ∼350–550 d post-explosion and hence does not require accurate constraints on the explosion epoch.

The sample of SN spectra used in this work is detailed in Section 2. The sample is a combination of IIP SNe found in the literature with good photometric and spectral coverage during the nebular phase, along with new previously unpublished observations. The photometric coverage was necessary so that the ^{56}Ni mass could be estimated independently from the spectra and an empirical relation between the ejected ^{56}Ni mass and the line widths could be determined. We have added one more IIP SNe with nebular phase observations and reliable ^{56}Ni mass estimates to the sample, SN 1997D, which was a low-luminosity, low-velocity SN with an ejected ^{56}Ni mass of 0.008 $M_\odot$ (Pastorello et al. 2004). SN 1997D is not studied in detail here because of the lack of information on its progenitor star. The spectra of SN 1997D are taken from Benetti et al. (2001) with a spectral resolution of 13 Å.

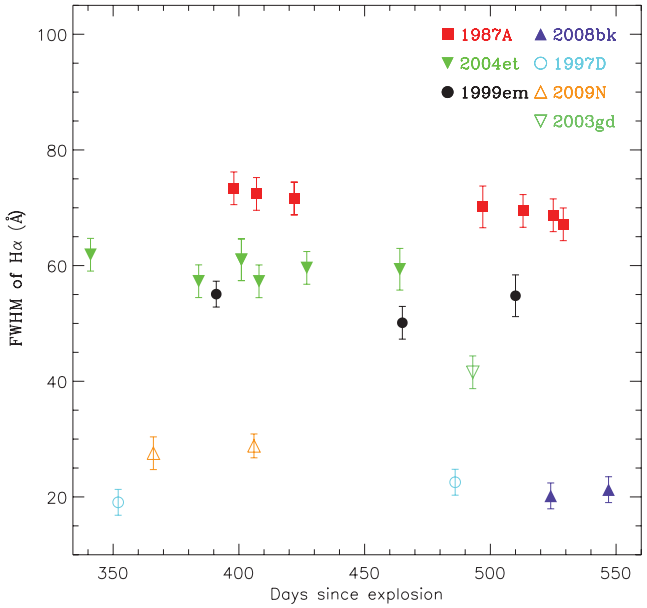

Figure 14. The $FWHM_{corr}$ of the Hα emission line corrected for the instrumental resolution for SNe 1987A, 1997D, 1999em, 2003gd, 2004et, 2008bk and 2009N as a function of time since explosion.

The FWHM of the most prominent feature in the spectra, the Hα 6563 Å emission line, was measured by fitting a Gaussian to the emission profile. This line is very strong in all the spectra and is unblended with other lines so we can be confident that the FWHM can be measured to good accuracy. As in Section 4.2, the FWHM of the line profiles were corrected for the spectral resolution of the instruments used to obtain each spectrum. Fig. 14 shows the $FWHM_{corr}$ of the Hα emission line as a function of time for eight IIP SNe that also have ^{56}Ni masses estimated from their bolometric light curves. From Fig. 14, it can be clearly seen that for any given SN, the $FWHM_{corr}$ is relatively constant at these epochs and so observations at a coeval epoch are unnecessary for a comparison to be made. A mean value of the $FWHM_{corr}$ was calculated for each SN from the available data at epochs in the range ∼350–550 d. These values can then be compared to the ^{56}Ni mass estimated from the luminosity of the nebular phase light curve. The $FWHM_{corr}$ value used for each SN along with its ^{56}Ni mass estimate from the literature is given in Table 5.

Fig. 15 shows the ejected ^{56}Ni mass calculated from the tail phase luminosity of the SNe against the $FWHM_{corr}$ of the Hα emission line. It is immediately apparent that a correlation exists between these parameters, with small $FWHM_{corr}$ (low-velocity) events such as SNe 1997D, 2008bk and 2009N displaying correspondingly smaller ^{56}Ni masses. In a similar way, the higher velocity SNe

Table 5. Data used for Fig. 15 to determine the relationship between the ejected ^{56}Ni mass and the FWHM of Hα corrected for the spectral resolution.

SN	$FWHM_{H\alpha}$ (Å)	^{56}Ni mass ($M_\odot$)	Reference
1997D	20 ± 4	0.008 ± 0.006	Benetti et al. (2001)
2008bk	21 ± 2	0.004 ± 0.003	Pignata et al. (in preparation)
2009N	28 ± 3	0.009 ± 0.004	Takáts et al. (in preparation)
2003gd	44 ± 5	0.016 ± 0.01	Hendry et al. (2005)
1999em	51 ± 2	0.036 ± 0.005	Utrobin (2007)
2004et	60 ± 2	0.064 ± 0.04	Maguire et al. (2010)
1987A	70 ± 4	0.069 ± 0.0012	Bouchet et al. (1991)

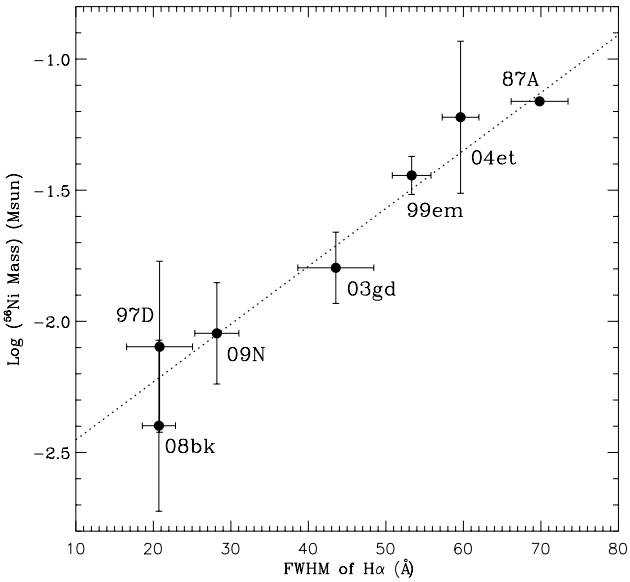

Figure 15. The ^{56}Ni mass obtained from the tail phase of the bolometric light curve against the FWHM of the Hα emission line for the SNe listed in Table 5.

of the sample, such as SNe 1987A and 2004et, have higher ^{56}Ni masses. The relationship between the mass of ejected ^{56}Ni and the $FWHM_{corr}$ of the Hα emission line can be fitted with an equation of the form

$$M(^{56}\mathrm{Ni}) = A \times 10^{B\ \mathrm{FWHM_{corr}}}\ \mathrm{M}_\odot, \quad (3)$$

where $B = 0.0233 \pm 0.0041$ and $A = 1.81^{+1.05}_{-0.68} \times 10^{-3}$. The reduced χ^2 value for this fit is 0.73. This equation can be used for SNe for which limited photometric data are available or where there are large uncertainties on the distance and extinction estimates.

As an example we apply this relation to two IIP SNe, without good late-time light curves. SN 2008cn is a IIP SN that was observed spectroscopically at the VLT at an epoch of +358 d post-explosion. No photometric data have yet been published on this object, but from our spectrum, using an $FWHM_{corr}$ of Hα of 79 Å, we have estimated the ^{56}Ni mass to be $0.13^{+0.30}_{-0.09}\,\mathrm{M}_\odot$. SN 2007aa is another IIP SN that was observed at the VLT at a nebular phase epoch of +376 d post-explosion and found to have for Hα an $FWHM_{corr}$ of 52 Å which gives a ^{56}Ni mass of $0.03^{+0.05}_{-0.02}\,\mathrm{M}_\odot$. Hopefully these ^{56}Ni mass estimates will be confirmed by future data releases for these SNe. The uncertainties in these estimates are relatively large, but at the very least this method can be used to determine between low, intermediate and high ejected ^{56}Ni masses. A larger sample is needed to study this method of ^{56}Ni mass determination in more detail and in particular it would be of interest to include some IIL SNe to see if the relation also holds for these events.

A correlation between the ^{56}Ni mass and explosion energy for IIP SNe was shown by Hamuy (2003) for a sample of 16 IIP SNe, with higher ^{56}Ni mass events having greater explosion energies. Nadyozhin (2003) also described a correlation between the explosion energy and the ^{56}Ni mass of IIP SNe, which was suggested to have a complex nature that also depends on the progentior mass. One can assume that the velocity (or equivalently the FWHM) of the line profiles will scale with the explosion energy (which is a combination of internal and kinetic energy), since the more energy produced in the explosion, the more kinetic energy that will be given to the ejecta [at least 90 per cent of the explosion energy (Arnett 1996)]. This is the first time a correlation between the FWHM of

the nebular phase line profiles and the ^{56}Ni mass has been identified, and assuming similar ejecta masses for the SN sample, can be interpreted as a correlation between the explosion energy and the ^{56}Ni mass.

8 SUMMARY AND CONCLUSIONS

In this paper we have investigated the nebular phase spectra of a sample of IIP SNe and compared their observational analysis to the detailed radiative transfer model to try to better understand the formation of the various emission lines and their variation within the sample. We have focused on IIP SNe with either progenitor detections or restrictive limits on their progenitor masses. Despite the large variation in ^{56}Ni masses and expansion velocities, the characteristics of the emission lines in the nebular spectra of IIP SNe are found to be relatively homogeneous and independent of progenitor masses. For each SN, the shapes of the different emission line profiles are very similar and suggest a similar spatial distribution of the different elements. This is also seen when the velocities of the prominent emission lines are measured using their HWHM, with only Hα showing a noticeably higher velocity, which suggests a larger contribution from farther out in the ejecta.

For SN 1987A, we found, as has been previously shown, that the Hα velocity was significantly larger than the [O I] velocity, while for the other SNe in our sample the differences between H and [O I] were not as pronounced. This suggests that the zones responsible for [O I] emission are different in the rest of the SN sample compared to those in SN 1987A. From the analysis of the line profiles and widths, it appears that all IIP SNe (excluding SN 1987A) have similar spatial distributions of [O I] which is closer in velocity to Hα than for SN 1987A. This implies that the [O I] flux could be predominantly emitted by primordial O in the H zones and may not be coming from the synthesized O from the inner regions of the ejecta. The line profiles are also shown to be intrinsically peaked in shape, even after taking into account the convolution with the instrumental resolution. This shows that mixing must have occurred for all the elements to be producing emission from both the centre and the outer regions of the ejecta.

These observational results are corroborated by the output of the radiative transfer model of a 12 $M_\odot$ star, where a significant proportion of the flux of the prominent emission lines is found to originate in the H-rich zones. For SN 1987A, the [Ca II] and several [Fe II] emission lines were also found to be predominantly formed in the H zones, but here we present the new result that for the 12 $M_\odot$ progenitor model used here, the [O I] flux is produced in approximately equal amounts by O in the H zones and O in the inner O-rich zones, and this explains the much smaller difference between the Hα and [O I] velocities seen for our sample of SNe. This has major implications for current methods of calculating the synthesized O mass in IIP SNe, which assume that the [O I] 6300, 6364 Å line emission is produced solely by synthesized O. A calculation of the synthesized O mass of SN 2004et that takes into account these new results will be presented in Jerkstrand et al. (in preparation).

The flux ratios of the emission lines from the 12 $M_\odot$ model were found, in general, to agree quite well with the observed flux ratios. No trends were found between the progenitor mass and the observed flux ratios, in agreement with the result that the flux in these lines has a significant contribution from primordial abundances. We also investigated possible correlations between the spectral properties and other observational properties of the SNe and found a correlation between the ejected ^{56}Ni mass and the FWHM of the Hα emission line. An empirical relation was obtained, which can be used to estimate the ^{56}Ni mass of SNe with limited bolometric coverage and/or poor constraints on their extinction and distance. The benefit of this method is that it requires only the width of the Hα emission line during the nebular phase to estimate the ^{56}Ni mass. Even more importantly, this provides a strong constraint on explosion models, particularly the amount of fall-back material in them.

ACKNOWLEDGMENTS

CF and AJ are supported by the Swedish Research Council and the Swedish National Space Board. SB, FB and AP are partially supported by the PRIN-INAF 2009 with the project 'Supernova variety and nucleosynthesis yields'. GL is supported by a grant from the Carlsberg foundation. The Dark Cosmology Centre is funded by the Danish National Research Foundation. This work made use of the code developed by Kozma & Fransson (1992) for the computation of the non-thermal electron degradation. This work has made use of data taken at the VLT under programme numbers 080.D-0213(B), 084.D-0261(B), 083.D-0131(B) and 084.D-0261(B) and at the NTT under programme numbers 083.D-0970(A) and 184.D-1140(S).

REFERENCES

Aitken D. K., Smith C. H., James S. D., Roche P. F., Hyland A. R., McGregor P. J., 1988, MNRAS, 237, 19
Andrews J. E. et al., 2010, ApJ, 715, 541
Andrews J. E. et al., 2011, ApJ, 731, 47
Arnett D., 1996, Supernovae and Nucleosynthesis: An Investigation of the History of Matter, from the Big Bang to the Present. Princeton Univ. Press, Princeton, NJ
Benetti S., Cappellaro E., Turatto M., della Valle M., Mazzali P. A., Gouiffes C., 1994, A&A, 285, 147
Benetti S. et al., 2001, MNRAS, 322, 361
Bersten M., Hamuy M., 2009, ApJ, 701, 200
Bouchet P., Danziger I. J., 1993, A&A, 273, 451
Bouchet P., Phillips M. M., Suntzeff N. B., Gouiffes C., Hanuschik R. W., Wooden D. H., 1991, A&A, 245, 490
Chornock R., Filippenko A. V., Li W., Silverman J. M., 2010, ApJ, 713, 1363
Chugai N. N., 1990, Sov. Astron. Lett., 16, L457
Chugai N. N., 1994, ApJ, 428, L17
Crockett R. M., Smartt S. J., Pastorello A., Eldridge J. J., Stephens A. W., Maund J. R., Mattila S., 2011, MNRAS, 410, 2767
Dessart L., Livne E., Waldman R., 2010, MNRAS, 408, 827
Dotani T., Hayashida K., Inoue H., Itoh M., Koyama K., 1987, Nat, 330, 230
Eldridge J. J., Tout C. A., 2004, MNRAS, 353, 87
Elias J. H., Gregory B., Phillips M. M., Williams R. E., Graham J. R., Meikle W. P. S., Schwartz R. D., Wilking B., 1988, ApJ, 331, L9
Elias-Rosa N. et al., 2009, ApJ, 706, 1174
Elmhamdi A., 2011, Acta Astron., 61, 179
Elmhamdi A. et al., 2003a, MNRAS, 338, 939
Elmhamdi A., Chugai N. N., Danziger I. J., 2003b, A&A, 404, 1077
Fassia A., Meikle W. P. S., Geballe T. R., Walton N. A., Pollacco D. L., Rutten R. G. M., Tinney C., 1998, MNRAS, 229, 150
Fransson C., Chevalier R. A., 1987, ApJ, 322, L15
Fransson C., Chevalier R. A., 1989, ApJ, 343, 323
Fransson C., Kozma C., 2002, New Astron. Rev., 46, 487
Graham J. R., 1988, ApJ, 335, L53
Hamuy M., 2003, ApJ, 582, 905
Heger A., Fryer C. L., Woosley S. E., Langer N., Hartmann D. H., 2003, ApJ, 591, 288
Hendry M. A. et al., 2005, MNRAS, 359, 906
Hirschi R., Meynet G., Maeder A., 2004, A&A, 425, 649
Inserra C. et al., 2011, MNRAS, 417, 261
Jerkstrand A., Fransson C., Kozma C., 2011, A&A, 530, A45

Kirshner R. P., Kwan J., 1975, ApJ, 197, 415
Kleiser I. K. W. et al., 2011, MNRAS, 415, 472
Kotak R. et al., 2009, ApJ, 703, 306
Kozma C., Fransson C., 1992, ApJ, 390, 602
Kozma C., Fransson C., 1998a, ApJ, 497, 431
Kozma C., Fransson C., 1998b, ApJ, 496, 946
Kumagai S., Shigeyama T., Nomoto K., Itoh M., Nishimura J. Tsuruta S., 1989, ApJ, 345, 412
Leonard D. C. et al., 2002, PASP, 114, 35
Li H., McCray R., 1992, ApJ, 387, L309
Li H., McCray R., 1993a, ApJ, 405, 730
Li H., McCray R., Sunyaev R. A., 1993b, ApJ, 419, 824
Li W., Van Dyk S. D., Filippenko A. V., Cuillandre J.-C., Jha S., Bloom J. S., Riess A. G., Livio M., 2006, ApJ, 641, 1060
Limongi M., Chieffi A., 2003, ApJ, 592, 404
Liu W., Dalgarno A., 1995, ApJ, 454, 472
Lucy L. B., Danziger I. J., Gouiffes C., Bouchet P., 1989, in Tenorio-Tagle G., Moles M., Melnick J., eds, Lecture Notes in Physics, Vol. 350, Proc. IAU Colloquium 120, Structure and Dynamics of the Interstellar medium. Springer-Verlag, Berlin, p. 164
Maeda K. et al., 2008, Sci, 319, 1220
Maguire K. et al., 2010, MNRAS, 404, 981
Mattila S., Smartt S. J., Eldridge J. J., Maund J. R., Crockett R. M., Danziger I. J., 2008, ApJ, 688, L91
Maund J. R., Smartt S. J., Danziger I. J., 2005, MNRAS, 364, L33
Meikle W. P. S., Allen D. A., Spyromilio J., Varani G.-F., 1989, MNRAS, 238, 193
Meikle W. P. S., Spyromilio J., Allen D. A., Varani G.-F., Cumming R. J., 1993, MNRAS, 261, 535
Meikle W. P. S. et al., 2007, ApJ, 665, 608
Meikle W. P. S. et al., 2011, ApJ, 732, 109
Milisavljevic D., Fesen R. A., Gerardy C. L., Kirshner R. P., Challis P., 2010, ApJ, 709, 1343
Modjaz M., Kirshner R. P., Blondin S., Challis P., Matheson T., 2008, ApJ, 687, L9
Nadyozhin D. K., 2003, MNRAS, 346, 97
Pastorello A. et al., 2004, MNRAS, 347, 74
Pastorello A. et al., 2005, MNRAS, 360, 950
Pastorello A. et al., 2009, MNRAS, 394, 2266
Phillips M. M., Hamuy M., Heathcote S. R., Suntzeff N. B., Kirhakos S., 1990, AJ, 99, 4
Pinto P. A., Woosley S. E., 1988, ApJ, 329, 820
Pozzo M. et al., 2006, MNRAS, 368, 1169
Sahu D. K., Anupama G. C., Srividya S., Muneer S., 2006, MNRAS, 372, 1315
Smartt S. J., 2009, ARA&A, 47, 63
Smartt S. J., Eldridge J. J., Crockett R. M., Maund J. R., 2009, MNRAS, 395, 1409
Spyromilio J., Pinto P. A., 1991, in Danziger I. J., Kjär K., eds, Proc. ESO/EIPC Supernova Workshop. ESO, Gording, p. 423
Spyromilio J., Meikle W. P. S., Learner R. C. M., Allen D. A., 1988, Nat, 334, 327
Sugerman B. E. K. et al., 2006, Sci, 313, 196
Sunyaev R. et al., 1987, Nat, 330, 227
Taubenberger S. et al., 2009, MNRAS, 397, 677
Thielemann F.-K., Nomoto K., Hashimoto M.-A., 1996, ApJ, 460, 408
Uomoto A., 1986, ApJ, 310, L35
Utrobin V. P., 2007, A&A, 461, 233
Utrobin V. P., Chugai N. N, 2009, A&A, 506, 829
Utrobin V. P., Chugai N. N., 2008, A&A, 491, 507
van Dyk S. D. et al., 2012, AJ, 143, 19
Walborn N. R., Lasker B. M., Laidler V. G., Chu Y.-H., 1987, ApJ, 321, 41
Wooden D. H., Rank D. M., Bregman J. D., Witteborn F. C., Tielens A. G. G. M., Cohen M., Pinto P. A., Axelrod T. S., 1993, ApJS, 88, 477
Woosley S. E., Heger A., 2007, Phys. Rep., 442, 269
Woosley S. E., Weaver T. A., 1995, ApJS, 101, 181
Xu Y., McCray R., Oliva E., Randich S., 1992, ApJ, 386, 181

This paper has been typeset from a TEX/LATEX file prepared by the author.